Accepted to Phys. Fluids 10.1063/5.0185472

Numerical investigation of a pair of in-line bubbles rising in Newtonian and non-Newtonian fluids with interfacial passive scalar transfer

Koorosh Kazemi,[1] Anton Vernet,[1] Francesc X. Grau,[1] Jordi Pallarès,[1] Alexandre Fabregat,[1, a)] and Salvatore Cito[1]

Departament d'Enginyeria Mecànica, Universitat Rovira i Virgili, Av. Països Catalans 26, Tarragona, 43007 (Spain)

We employ three-dimensional, fully-resolved numerical simulations using the Volume-of-Fluid (VOF) method to study the motion and interaction of two in-line bubbles ascending in both Newtonian and shear-thinning fluids. Additionally, we explore passive scalar transfer between the fluid phases across a variety of fluidic conditions, modeling shear-thinning behavior in non-Newtonian fluids through the Carreau model. The impact of the Galilei (Ga) and Bond (Bo) numbers, bubble pair radius ratio, inelastic time constant (λ), and flow index (n) on the bubbles dynamics and transient Sherwood number (Sh_t) and surface-averaged Sherwood number ($\langle Sh \rangle$) are reported. Using the well-known $Ga - Bo$ regime phase diagram for a single rising bubble in a Newtonian ambient fluid, the present numerical experiments are used to study the departure from this reference case due to the presence and characteristics of a second bubble and the non-Newtonian nature of the ambient fluid. When categorized based on the single bubble phase diagram, we found that in Regimes I (axisymmetric) and III (oscillatory), a pair of bubbles doesn't break up or merge during our simulations. However, their behaviors vary due to the second bubble and changes in non-Newtonian fluid parameters like the inelastic time constant and flow index. Likewise, we explored this parameter space for Regime II (skirted), where the two bubbles eventually merge, and Regimes IV (peripheral breakup) and V (central breakup), known for multiple bubble breakups. Additionally, we present results on differently sized bubbles, showing that their merging tendency depends on their arrangement as leading or trailing positions in the pair.

Keywords: Bubble rising; Newtonian fluid; Shear-thinning fluid; Mass transfer

[a)]Electronic mail: alexandre.fabregat@urv.cat

Accepted to Phys. Fluids 10.1063/5.0185472

I. INTRODUCTION

Fluid systems containing bubbles are widely observed in natural phenomena such as breaking waves[1] and in a wide range of engineering applications including bubble column reactors[2] and heat exchangers[3]. Momentum and heat/mass transfer between the bubbles and the surrounding fluids are common phenomena in many industrial processes including chemical reactors based on bubbly flow[4], multiphase cooling systems[5], wastewater treatment[6], metal refining[7] and also in nature such as bubbly plumes under the oceans[8].

Buoyancy-driven bubbly flows are widely used in industrial applications to enhance heat/-mass transfer. The effectiveness of this heat/mass transfer depends on the complex interplay of factors such as flow behavior, bubble distributions, interactions, and interfacial transport mechanisms. To accurately predict heat/mass transfer rates, it is essential to consider advection, diffusion, and transfer across bubble interfaces. However, predicting heat/mass transfer is challenging due to complex interactions between bubbles, deformable bubble interfaces, and significant differences in diffusion coefficients between the phases. One of the primary motivations of this study is to gain a deeper understanding of bubble interactions in bubbly flows. These interactions can lead to important physical processes such as coalescence and breakup, which can significantly impact the heat/mass transfer rate by altering interfacial area. Studying the evolution, flow dynamics, and scalar transport in a simplified system of two bubbles provides a valuable platform for understanding the fundamental mechanisms governing bubbly flows. The insights gained from this study will be crucial for designing gas-liquid equipment that optimizes heat/mass transfer efficiency. By developing a comprehensive understanding of bubble dynamics, especially interactions between bubbles, we can develop more accurate models for predicting heat/mass transfer rates in bubbly flows and enhance the performance of industrial processes.

The dynamics of a pair of bubbles rising has been experimentally studied under different conditions. Bhaga and Weber[9] performed experiments on two bubbles rising in line in a viscous liquid measuring the velocity in the wake of the bubbles and presenting a correlation for the wake velocity over a range of Reynolds number ($10 < Re < 100$). Katz and Meneveau[10] experimentally measured the rising velocity of the bubble pairs rise in water with different initial separations and different bubble sizes at the Reynolds number ranging between 0.2 and 35 and Bond numbers (Bo) of less than 0.3. Watanabe and Sanada[11] inves-

tigated the motion of a pair of bubbles both numerically and experimentally showing that at moderate Reynolds numbers ($5 < Re < 150$) there is an equilibrium distance between bubbles although it is unstable due to 3D effects. Sanada et al.[12] experimentally studied the coalescence of a pair of bubbles rising in silicone oil and water side by side investigating the critical Reynolds number and Weber number for bouncing of the bubbles. They also showed that the rising velocity of the bubbles decreases after coalescence. Kusuno and Sanada[13] experimentally investigated a pair of bubbles rising in line in ultrapure water at intermediate Reynolds number ($50 < Re < 300$) introducing a correlation for drag coefficient of a solitary bubble for different Re. They also studied the effects of the bubble radius on the bubbles dynamics showing that there are four different types of motion including separating, approaching, coalescing, and overtaking. Kusuno et al.[14] experimentally investigated the dynamics of two clean air bubbles rising in line in silicone oil estimating the drag and lift coefficients for the Reynolds number ranged from 20 to 60.

With rapid growth and development of numerical methods, and due to the limitations and restrictions of the experiments, numerical simulation has become a powerful tool to reach in-demand characteristics and behavior of the bubble rising and bubbles interaction mechanism in different surrounding fluids. Yuan and Prosperetti[15] performed a numerical investigation on an undeformable axisymmetric pair of bubbles rising in line in a viscous fluid at Reynolds number up to 200 using a mixed spectral/finite-difference scheme. They showed that there is a stable equilibrium distance between the bubbles due to a balance between the wake effect and inertial repulsion. Chen et al.[16] used a modified Volume-of-Fluid (VOF) method to simulate the motion of a pair of initially spherical bubbles rising at Reynolds number up to 200 and two different Bond numbers (50 and 420) studying the effect of initial separation on the bubbles dynamics. They found that the bubbles merge for small values of initial separation while for large values the bubbles do not merge. Hasan and Zakaria[17] simulated the coalescence process of two in-line bubbles using VOF with two different Reynolds numbers (8.5 and 10) and four different Bond numbers (4.25, 5, 42.5, and 50) showing that the high surface tension force postpones the coalescence for a fixed value of density and viscosity ratios. Chen et al.[18] carried out a two-dimensional numerical simulation of a pair of bubbles rising in line and also side by side in a liquid pool using the moving particle semi-implicit (MPS) method. They studied the effects of the bubble radius on the bubbles dynamics and coalescence showing that the coalesced

bubble rises with volume and velocity oscillations and the time of the volume oscillations increase by increasing the bubble radius. Tripathi et al.[19] numerically studied two bubbles rising side by side in quiescent liquid considering six different $Ga - Bo$ sets as $(Ga, Bo) = (22.4, 4), (32, 4), (60, 4), (25, 1), (100, 2)$, and $(25, 4)$. They investigated the effects of Ga, Bo, and initial separation on the bubbles dynamics and showed that there is a mirror symmetry in the trajectories of the bubbles even in a high-inertia regime (high Ga). Zhang et al.[20] used axisymmetric computations to investigate the coalescence and interaction of two bubbles rising in line in viscous liquids. They studied the effects of surrounding fluid viscosity on the coalescence proposing a bifurcation diagram that shows four different coalescence regimes. Cao and Macián-Juan[21] performed a numerical simulation of two in-line bubbles rising in quiescent liquid to study the effects of initial separation on the bubbles dynamics. They noted that at a small initial separation, the trailing bubble collides with the leading bubble and a central breakup of the trailing bubble due to the elongation is observed. They also showed that at larger initial separation, the trailing bubble has lateral motion due to the leading bubble wake. The coalescence and interaction of two in-line bubbles rising in quiescent liquid were also numerically studied by Kumar et al.[22]. They investigated the effects of initial separation and ratio of the bubbles radius on the coalescence showing that the coalescence time increases by increasing the initial separation.

A significant part of studies in the literature focused on the bubble rising in Newtonian fluids while many materials encountered in both nature and industry are non-Newtonian fluids such as blood, polymers and carboxymethyl cellulose (CMC) solutions. Bubble rising behavior and interactions in non-Newtonian fluids are more complex compared to Newtonian fluids and also relevant research is quite rare. Rodrigo Vélez-Cordero et al.[23] carried out experiments on a pair of bubbles rising in Xanthan gum with flow indexes (n) of 0.85 and 0.55 showing that with decreasing the flow index, the wake formed behind the leading bubble attracts the trailing bubble faster. Fan and Yin[24] performed a numerical simulation to study the interaction of two bubbles rising in shear-thinning fluids, presented by the power-law model, using VOF method coupled with the Continuous Surface Force (CSF) method. They considered different bubbles configurations (side-by-side and oblique) and different initial separations showing that for side-by-side bubbles, the repulsive effect decreases with the initial separation, and for two oblique bubbles, there might exist an equilibrium angle at which the repulsive and attractive interactions are balanced. Oblique and side-by-side

configurations for a pair of bubbles rising in shear-thinning fluids modeled by the power-law also were numerically studied by Tariqul Islam et al.[25] using VOF method. They pointed out that by decreasing the flow index, the shape of the bubbles changes from spherical to irregular and also considerable oscillation happens between the bubbles. Liu et al.[26] applied VOF simulations to study the coalescence and interaction of multiple horizontal bubbles rising in shear-thinning fluids with different arrangements and initial separations obtaining the critical bubble separation for coalescence under various conditions. Sun et al.[27] studied the dynamical behavior of multiple bubbles rising in shear-thinning fluids with equilateral triangle arrangement at Reynolds number ranged from 5 to 300 introducing the correlation of the interaction coefficient among the bubbles as the ratio of the bubble drag coefficient for multiple systems and a single bubble rising under same conditions. They[28] also used VOF method to simulate three horizontal bubbles with different sizes in shear-thinning fluids proposing a correlation for the drag coefficient of the bubbles.

The literature provides complete research on heat/mass transfer across a single bubble interface[29]. However, in industrial applications, multiple bubbles are more commonly encountered than a single bubble and the interactions between the bubbles affect the heat/mass transfer remarkably. As the bubbles rise in gas-liquid systems, the coalescence and breakup occur repeatedly since the bubbles contact each other. Thus, the interfacial area of the bubbles alters as well as the rising velocity which leads to a change in heat/mass transfer rate.

In this paper, we conduct a numerical study on the motion, interaction and passive scalar transport for a pair of in-line bubbles rising in Newtonian and shear-thinning fluids with different sets of (Ga, Bo) investigating the effects of Ga, Bo, the bubble pair radius ratio, the flow index (n), and the inelastic time constant (λ).

II. PHYSICAL MODEL

Fig. 1 shows a diagram of the numerical domain consisting of a cubic box filled with a Newtonian or non-Newtonian fluid with a non-dimensional length of 120 while the length scale of the problem is $d = 2R$ where R is the radius of the spherical leading bubble (LB) and trailing bubble (TB). In the simulation domain, defined as a cubic box with $-60 < x < 60$, $0 < y < 120$, and $-60 < z < 60$, the initial positions of the center of leading bubble (LB)

Accepted to Phys. Fluids 10.1063/5.0185472

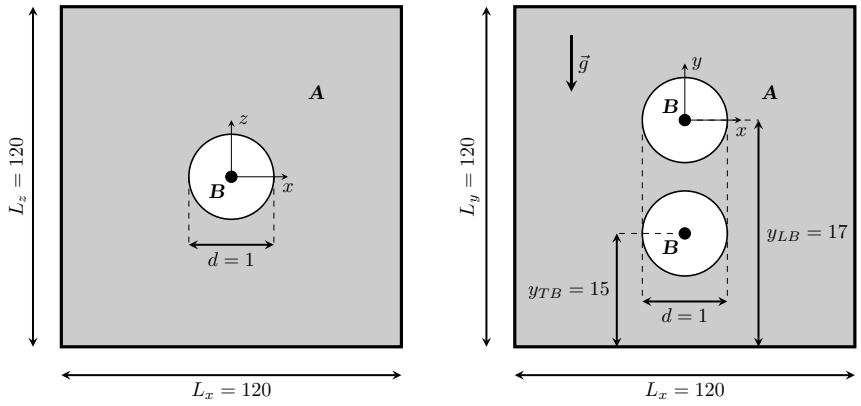

FIG. 1. Top and side views of the computational domain (not to scale) showing the flow configuration with initially spherical bubbles of fluid B and non-dimensional diameter $d = 1$; one placed at $y_{TB} = 15$ and another placed at $y_{LB} = 17$ in a $L_x = L_y = L_z = 120$ cubical box filled with fluid A.

and trailing bubble (TB) are $(x_{\mathrm{LB}}, y_{\mathrm{LB}}, z_{\mathrm{LB}}) = (0, 17, 0)$ and $(x_{\mathrm{TB}}, y_{\mathrm{TB}}, z_{\mathrm{TB}}) = (0, 15, 0)$, respectively. Both bubbles start with zero velocity. The large box dimensions ensure that the wall effects on the bubble dynamics are minimized. The initial separation between the center of the bubbles, s, for all cases is $4R$, and the Peclet number ($Pe = \frac{u^* l^*}{\mathcal{D}}$) of the gas bubbles is fixed at 1000 while for the surrounding fluid, it is fixed at 10^7. In this context, $\mathcal{D}$ represents the scalar diffusion coefficient of fluid B and the scales for length and velocity are denoted as $l^* = R$ and $u^* = \sqrt{gR}$, respectively. The values of λ and n for the shear thinning fluids used in this paper are taken from the experiments of Zhang et al.[30] and also numerical simulations of Premlata et al.[31] and Cano-Lozano and Martínez-Bazán[32] and their ranges are $2 < \lambda < 10$ and $0 < n < 1$.

III. MATHEMATICAL AND NUMERICAL MODEL

Non-dimensional equations of mass and momentum conservation for incompressible binary and immiscible flows can be written as:

$$\nabla \cdot \mathbf{u} = 0, \tag{1}$$

$$\frac{D\mathbf{u}}{Dt} = \frac{1}{\alpha}\left[-\nabla p + \frac{1}{Ga^0}\nabla\cdot(\beta\nabla\mathbf{u}) + \frac{1}{Bo}\delta\kappa\vec{\mathbf{n}}\right] - \boldsymbol{\jmath}, \tag{2}$$

where $\alpha = \frac{\rho}{\rho_A}$, and $\beta = \frac{\mu}{\mu_A}$. Here, $\mathbf{u} = (u, v, w)$, p and t denote the non-dimensional velocity vector, pressure and time, respectively; wherein u, v and w represent the velocity components in the x, y and z directions, respectively. δ is the Dirac delta function, σ and g denote surface tension and gravitational acceleration, respectively. $Ga^0 = \frac{\rho_A g^{1/2} R^{3/2}}{\mu_A^0}$ and $Bo = \frac{\rho_A g R^2}{\sigma}$ denote initial Galilei number and Bond number, respectively, where R represents the radius of the initially spherical leading bubble. Here, A refers to the surrounding fluid phase and B represents the gas bubble phase. $\vec{\mathbf{n}}$ represents the outward-pointing unit normal to the surrounding fluid (fluid A) at the interface, $\kappa\vec{\mathbf{n}}$ denotes interfacial curvature and $\boldsymbol{\jmath}$ is the unit vector in the vertical direction (along gravity- negative y direction). Here, the surface tension force is considered as a body force term using the continuum method suggested by Brackbill et al.[33]. For two-phase flows, the density, ρ, and dynamic viscosity, μ, can be written as:

$$\rho \equiv \rho(f) = \rho_A f + \rho_B(1-f), \tag{3}$$

$$\mu \equiv \mu(f) = \mu_A f + \mu_B(1-f). \tag{4}$$

Here, f is the volume fraction of fluid ranging from 0 (phase B) to 1 (phase A) and it is used to track the interface between two phases. Specifically, the interface of the bubble is considered when the volume fraction reaches 0.5. The gas phase (fluid B) is considered to be Newtonian with a constant value of dynamic viscosity, μ_B, while the surrounding fluid (fluid A) can be Newtonian or shear-thinning fluid. For non-Newtonian fluids, the Carreau rheological model can be written as[34]:

$$\mu_A = \mu_A^0 \eta = \mu_A^0\left[1 + (\lambda\Pi)^2\right]^{(n-1)/2}, \tag{5}$$

where μ_A^0 represents the dynamic viscosity of fluid A corresponding to the zero shear rate. λ and n are the inelastic time constant and the flow index, respectively. $\Pi = (E_{ij}E_{ij})^{0.5}$ is the second invariant of the strain rate tensor, wherein $E_{ij} = \frac{1}{2}(\frac{\partial u_i}{\partial x_j} + \frac{\partial u_j}{\partial x_i})$. In this study, the values of density ratio, $\rho^\star(\equiv \frac{\rho_B}{\rho_A})$, and viscosity ratio, $\mu^\star$ $(\equiv \frac{\mu_B}{\mu_A^0})$, are set to 0.001 and 0.01, respectively.

The non-dimensional equation for the transport of a passive scalar, ϕ, can be written as:

$$\frac{\partial \phi}{\partial t} + \nabla \cdot \mathbf{u}\phi = \frac{1}{Pe}\nabla^2 \phi. \tag{6}$$

Here, $Pe = \frac{u^* l^*}{\mathcal{D}}$ is Peclet number. The initial value of ϕ inside the bubbles is 1 and everywhere else is zero.

To simulate the problem numerically, we used the Volume-of-Fluid (VOF) open-source solver *Basilisk*[35], which is a powerful multiphase CFD code[36,37] able to minimize parasitic currents at the interface[38]. Within the oct-tree mesh hierarchy of the solver, the background mesh resolution was set at 32 cells in each direction. Employing mesh refinement caused a notable surge in the total cell count, occasionally exceeding 5.5×10^7 cells, notably observed in regime V during later evolutionary phases. Examining the temporal progression of the dimensionless velocity magnitude $\|V\|$ and the transient Sherwood number $Sh_t = \frac{q_\phi}{\phi_0}$, where q_ϕ signifies the density flux and ϕ_0 denotes the initial value of the passive scalar, Fig. 2 illustrates the outcomes of mesh-independence investigations for a pair of bubbles rising with $Ga = 100$, $Bo = 100$, and $n = 0.5$. The variations observed among three distinct mesh levels ($m = 10, 11, 12$) imply that a mesh level of $m = 11$ achieves a satisfactory resolution. The parameter m represents the refinement level applied to the initial mesh resolution, determined by local values of velocity magnitude, passive scalar concentration, and bubble interface position.

Accepted to Phys. Fluids 10.1063/5.0185472

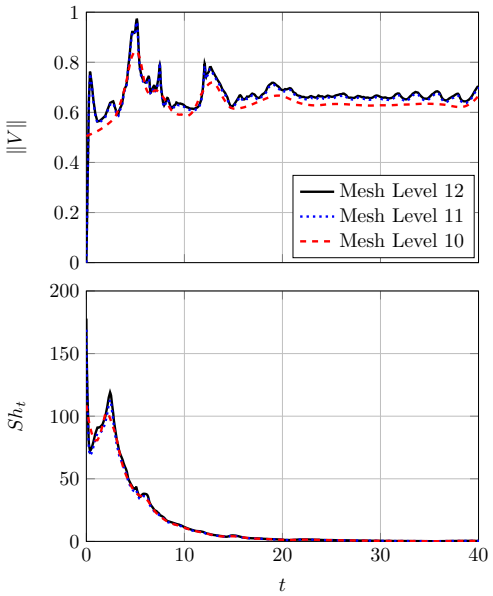

FIG. 2. Evolution of velocity magnitude (top) and transient Sherwood number (bottom) for a pair of bubbles rising in the shear-thinning fluid under conditions of (Ga,Bo)=(100,100) for different mesh levels.

The mass conservation error is quantified by examining the variation in the bubble volume through the following expression:

$$\mathcal{E} = 100\frac{\mathcal{V}(t) - \mathcal{V}_0}{\mathcal{V}_0} \tag{7}$$

Here, $\mathcal{V}_0$ denotes the initial volume of the bubble, and $\mathcal{V}(t) = (1-f)\int_V dV(t)$. The results depicted in Fig. 3 indicate that, even in scenarios characterized by numerous breakups and the formation of satellites ((Ga, Bo)=(100,100), $n = 0.5$), the error remains below 0.05%.

Accepted to Phys. Fluids 10.1063/5.0185472

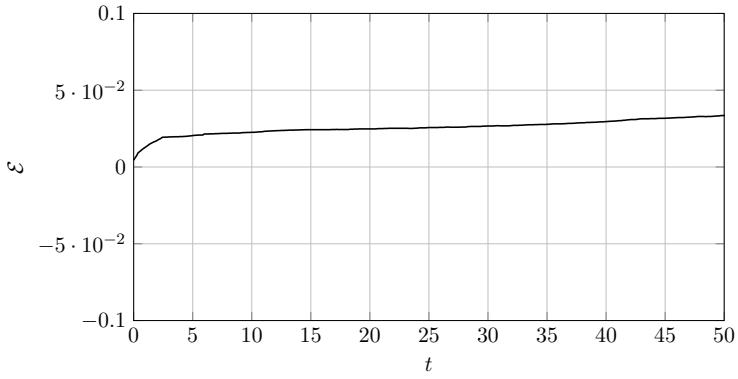

FIG. 3. The mass conservation error versus time.

In the Basilisk solver, the time-step independence is inherently managed through the Courant-Friedrichs-Lewy (CFL) condition, which dynamically adjusts the time step to ensure numerical stability. This adaptive time-stepping mechanism contributes to the reliability of our simulations, as it optimally aligns with the evolving dynamics of two in-line bubbles in diverse fluidic conditions.

Details of the non-dimensional analysis, derivations of the equations, and numerical method can be found in Kazemi et al.[39].

IV. VALIDATION OF NUMERICAL APPROACH

The methodology previously used to investigate the passive scalar transfer across the interface of a single bubble rising in Newtonian and non-Newtonian fluids[39] is validated here for the case of two in-line bubbles rising in a quiescent liquid with an initial separation of $S = 3R$. The present results are compared to experiments and numerical simulations previously reported in the literature. The Galilei, Bond and density and dynamic viscosity ratios are identical to those used in the experiments by Brereton and Korotney[40] who used $Ga = 23.78$, $Bo = 4$, and $\rho^\star = \mu^\star = 0.01$. Fig. 4 shows the coalescence process of the bubbles compared with experimental observations of Brereton and Korotney[40] and numerical results of Chakraborty et al.[41].

Although numerical and experimental results agree fairly well, the lag existing between

Accepted to Phys. Fluids 10.1063/5.0185472

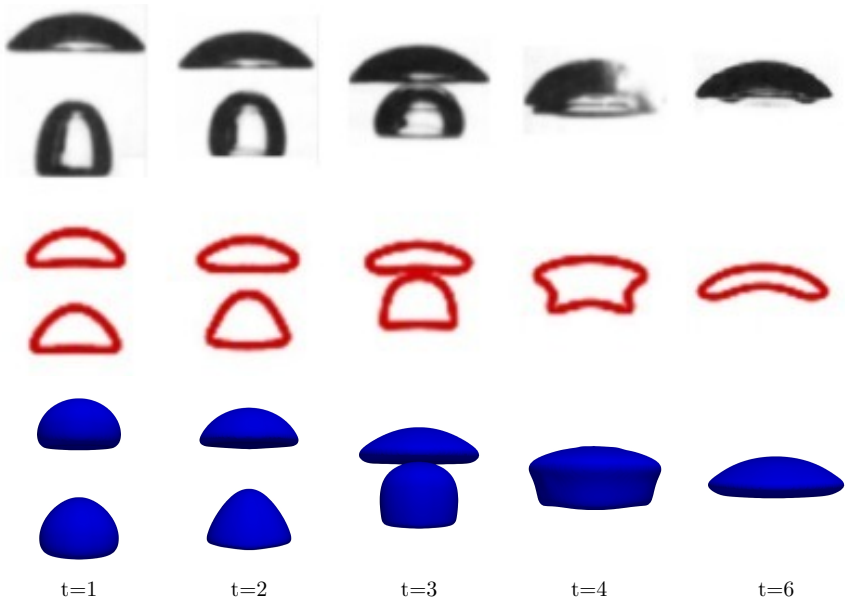

FIG. 4. The evolution of bubble shapes and the coalescence process. Top: Experimental observations of Brereton and Korotney[40]; Middle: Numerical results of Chakraborty et al.[41]; Bottom: Present work.

the two bubbles release times in the experiments along with minor departures from the spherical shape lead to distinct wake characteristics in comparison to the numerical simulations where bubbles are perfectly spherical and simultaneously released in a totally quiescent ambient fluid. Our results are also compared with those of Chakraborty et al.[41] who used coupled level-set and volume of fluid (CLSVOF) to simulate the same case in a two-dimensional domain. Using the instantaneous Reynolds number Re for the leading (LB) and trailing (TB) bubbles (based on the initial diameter and instantaneous rising velocity, $Re = \frac{\rho_A u_b R}{\mu_A^0}$), Fig.5 shows the comparison between the present and the Chakraborty et al.[41] methodologies. Results suggest that, despite the differences between the two numerical approaches, both simulations predict similar evolution of the Re number up to the quasi terminal conditions when this parameter plateaus at $Re = 49.1$, a value very close to the experimental value of $Re = 50$ obtained from the bubble diagram of Bhaga and Weber[42] and Clift et al.[43]. Regarding the interface scalar transport, validation results were presented

Accepted to Phys. Fluids 10.1063/5.0185472

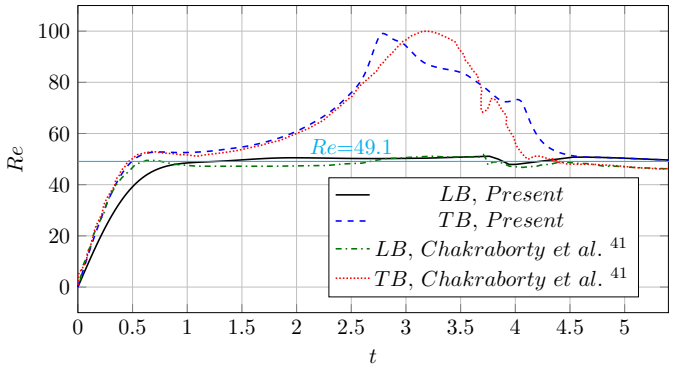

FIG. 5. Evolution of the instantaneous Re for the trailing and leading bubbles; Present work and numerical results of Chakraborty et al.[41].

and discussed in Kazemi et al.[39].

V. RESULTS AND DISCUSSION

We have simulated a pair of bubbles rising in line in a large tank containing either a Newtonian or a shear-thinning ambient fluid and studied the effects of different parameters on the dynamics of the bubbles and the passive scalar transfer across the interface of the bubbles. Specifically, we investigated the effects of the Ga and Bo numbers, the bubble pair radius ratio, the inelastic time constant λ, and the flow index n.

Depending on the flow set-up configuration and conditions, the dynamics of the pair of in-line bubbles is known to exhibit a few distinct motion patterns including: (i) side escape, (ii) Drafting-Kissing-Tumbling (DKT), and (iii) coalescence. In the side escape scenario, the sheltering effect induced by the LB results in an initial increase in the rising velocity of the TB, which eventually deviates from its vertical trajectory and escapes laterally from the wake of the LB. In DKT scenario, similarly to the side escape, the TB rising velocity exceeds that of the LB (drafting). However, instead of a sideways displacement with respect to the vertical path, the TB eventually touches (kissing) the LB and then rotates (tumbling) so that both bubbles keep rising in a side-by-side configuration. In the coalescence scenario, the sheltering effect of the LB again causes an increase in the rising velocity of the TB that eventually catches up with the LB so that both bubbles merge into a single body that

continues to rise.

A. Effects of Ga and Bo

The regime and trajectory of a single spherical air bubble rising in water are shown in a $Ga - Bo$ phase plot in Fig. 6. As can be seen, there are five different regimes including I. axisymmetric, II. skirted, III. oscillatory, IV. peripheral breakup, and V. central breakup.

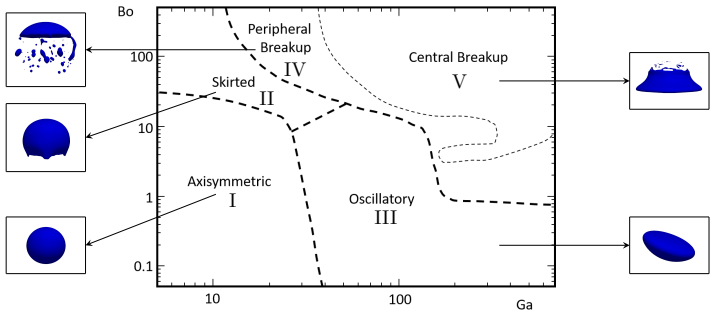

FIG. 6. $Ga - Bo$ phase plot of an air bubble rising in water. This figure is adapted from Tripathi et al.[44].

In this section, we have studied the effects of Ga and Bo numbers on the dynamical behavior of two in-line bubbles rising in Newtonian ($n = 1.0$) and shear thinning ($n = 0.5, \lambda = 6$) fluids and on the passive scalar transfer from the bubbles into the surrounding fluid. To this end, five different sets of (Ga, Bo) corresponding to different regimes have been considered: I. $(10, 1)$, II. $(10, 100)$, III. $(50, 2)$, IV. $(30, 100)$, and V. $(100, 100)$.

1. Dynamics of the bubbles

In regime I, since the buoyant force is dominant, a single bubble (SB) in a Newtonian fluid rises vertically with little deformation, preserving its axisymmetry, while in regime III, the SB displays oscillatory behavior, following a zigzag or spiral path during its ascent. In Regime III, the Galilei number is relatively high ($Ga > 30$), and the Bond number is relatively small ($Bo < 5$). This indicates a notable influence of gravitational forces compared

to viscous forces, and importantly, the surface tension forces are on a comparable scale to gravitational forces. These conditions uphold the drop shape, and the coming forces result in significant fluid acceleration and drag fluctuations around the bubble, leading to observable oscillatory behavior. A pair of bubbles, depending on the initial vertical separation between them, might exhibit much richer dynamics as a result of the sheltering effects interactions. These effects can be quantified by computing the instantaneous relative position of the bubbles in y-direction as $di_y = y_{LB} - y_{TB}$.

Figs. 7(a) and 7(b) present a series of instantaneous snapshots illustrating the bubble interfaces and accompanying streamlines of the background flow in regime I and regime III, respectively. The top row in each figure corresponds to the shear-thinning case, while the bottom row represents the Newtonian case.

In regime I, both pairs of bubbles exhibit similar initial rising behavior despite their different rheological properties. They follow a comparable trajectory until instability in the wake of the leading bubble causes a lateral shift. In the shear-thinning case, the faster trailing bubble eventually escapes from the leading bubble's wake, resulting in a quasi-steady side-by-side configuration with similar velocities, following the side escape scenario.

Conversely, in the Newtonian case, the drafting phase lasts until the trailing bubble catches up and "kisses" the leading one. They then rise together in a straight line until lateral separation occurs due to transverse flow disturbances. The trailing bubble subsequently rotates (tumbling) and breaks free from the leading bubble's wake, establishing a side-by-side arrangement and continuing to rise at comparable speeds, corresponding to the DKT scenario. The shear-thinning phenomenon causes viscosity to decrease as shear rate increases. As the faster-moving trailing bubble generates elevated shear rates around itself, the local viscosity diminishes. TB departures from the wake of LB due to the asymmetry in the wake flow field, creating conditions of varying viscosity for the TB. In Newtonian fluids, where the shear-thinning effect is absent, buoyancy and drag forces play a more prominent role. The slower movement of the trailing bubble in comparison to the shear-thinning case leads to contact with the leading bubble, initiating the DKT scenario. Following contact, transverse disturbances induce rotation and subsequent escaping of the trailing bubble.

In regime III, the shear-thinning case displays the side escape scenario, where the bubbles ascend in a zigzag path at nearly similar speeds after escaping. On the other hand, the Newtonian case follows the DKT scenario, with the pair of bubbles rising vertically after

Accepted to Phys. Fluids 10.1063/5.0185472

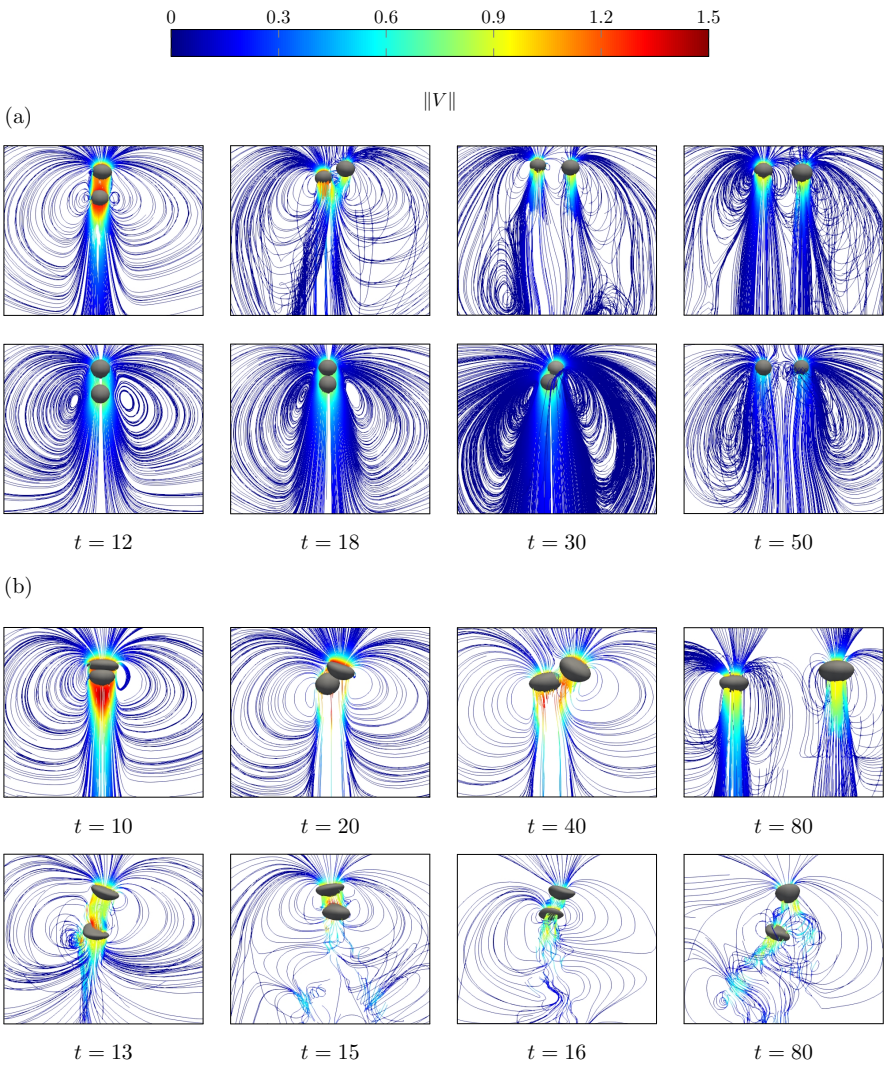

FIG. 7. Streamlines and shape of the bubbles in (a) regime I with (Ga,Bo)=(10,1), and (b) regime III with (Ga,Bo)=(50,2). In each panel: top: shear-thinning case ($n = 0.5$, $\lambda = 6$), and bottom: Newtonian case ($n = 1.0$). The colored map represents the non-dimensional non-dimensional velocity magnitude.

tumbling. Interestingly, the behavior of the pair of bubbles rising in the shear-thinning fluid in regime III is comparable to that of a single bubble rising in a Newtonian fluid, as both exhibit oscillatory behavior. However, in the Newtonian fluid, the pair of bubbles eventually rises vertically after a brief transition period. In Regime III, the elevated initial Galilei number implies stronger gravitational forces, contributing to a swifter ascent of bubbles compared to Regime I. Notably, in the shear-thinning case, the local Galilei number surpasses that of the Newtonian case due to reduced viscosity around the bubble. This reduction in viscosity in shear-thinning fluids results in a higher local Galilei number, leading to increased rising velocities and a distinctive zigzag trajectory. The larger Galilei number in shear-thinning conditions, compared to both the Newtonian case and Regime I, stems from a combination of heightened gravitational forces (in contrast to Regime I) and diminished viscous forces (compared to the Newtonian case). This interplay fosters pronounced fluid acceleration and disturbances around the bubble, giving rise to oscillatory behavior. Conversely, in the Newtonian case, the trailing bubble experiences a slower rising velocity compared to the shear-thinning case. This results in the adoption of the DKT scenario, where after escaping, the bubbles continue their ascent in a predominantly vertical path. The smaller local Galilei number in the Newtonian case, relative to shear-thinning conditions, contributes to this slower velocity and reduced disturbances around the bubbles. The nuanced balance between gravitational and viscous forces elucidates the contrasting dynamics observed between shear-thinning and Newtonian fluids in Regime III.

In Regime II, a single spherical bubble in a Newtonian fluid maintains a characteristic final shape known as "skirted" primarily due to the low surface tension. The surface tension of the fluid plays a crucial role in shaping the bubble. When surface tension is low, the forces acting on the bubble favor the formation of a broader, skirted shape. In this regime, the diminished surface tension allows the bubble to spread out and prevents the formation of a compact spherical shape. Surface tension tends to minimize the surface area of a bubble, favoring a spherical shape when it is high. However, in the case of low surface tension, the minimizing effect is less pronounced, and the bubble is more prone to adopting a broader and flattened configuration. The specific dynamics and equilibrium shape are a result of the delicate balance between various forces, including buoyancy, surface tension, and gravitational forces, and are particularly influenced by the level of surface tension in the fluid. In this particular regime, as the gravitational force is relatively low, the occurrence of

Accepted to Phys. Fluids 10.1063/5.0185472

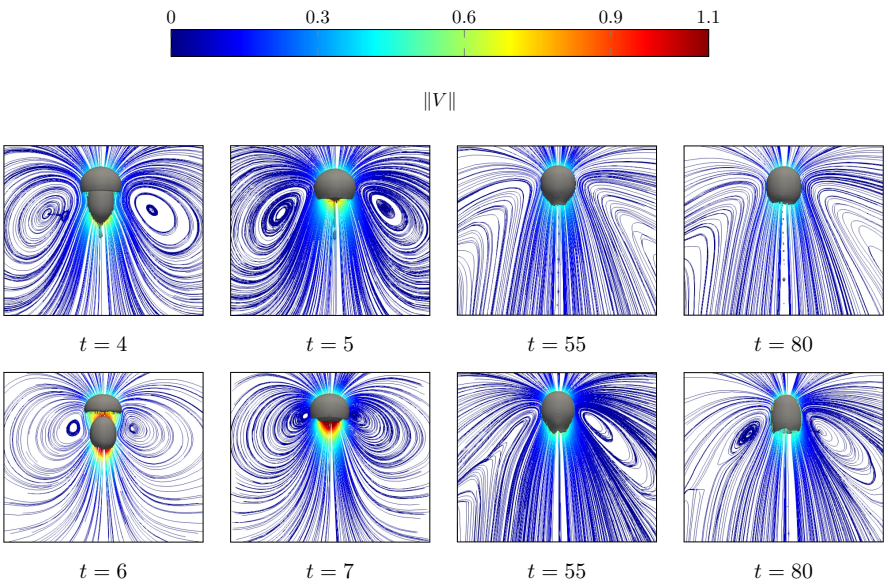

FIG. 8. Streamlines and shape of the bubbles in regime II with (Ga,Bo)=(10,100). Top: shear-thinning case ($n = 0.5$, $\lambda = 6$), and bottom: Newtonian case ($n = 1.0$). The colored map represents the non-dimensional velocity magnitude.

bubble breakup is minimized. Remarkably, as shown in Fig. 8, the bubble pair, regardless of rheology, also exhibits the same "skirted" topology as shown in Fig. 6 for a single bubble. At $(Ga, Bo) = (10, 100)$, the bubble pair coalesces into a single merged bubble (MB), continuing to evolve as expected based on Fig. 6.

When considering the influence of rheology, the time to coalescence decreases in the shear-thinning case compared to the Newtonian case. This discrepancy arises from the impact of shear-thinning rheology on the interaction between the leading and trailing bubbles. The sheltering effects generated by the wake of the leading bubble prompt accelerated motion of the trailing bubble in the shear-thinning case, causing quicker coalescence compared to the Newtonian case. Consequently, at a specific point in time, approximately $t \approx 5$ for shear-thinning and $t \approx 7$ for Newtonian, the two bubbles merge into a single entity. In the shear-thinning case, the merged bubble exhibits Galilei and Bond numbers of approximately $Ga \approx 14$ and $Bo \approx 160$, respectively, aligning with Regime II observed in a single bubble

rising in a Newtonian fluid.

The occurrence of peripheral breakup in a single bubble within Regime IV, characterized by a relatively high Bond number and a moderate Galilei number, can be attributed to the complex interplay of gravitational, inertial, and surface tension forces. In this regime, the balance between these forces leads to distinctive bubble behaviors. A relatively high Bond number implies that gravitational forces dominate over surface tension forces and the moderate Galilei number representing the ratio of inertial forces to gravitational forces, indicates a moderate influence of inertial forces on the bubble dynamics. Under these conditions, the gravitational forces acting on the bubble are strong enough to cause significant elongation, but not strong enough to overcome the stabilizing effects of surface tension entirely. Consequently, the bubble undergoes peripheral breakup, where the elongated portion of the bubble's periphery experiences instabilities leading to the formation of smaller satellite droplets. This phenomenon is a result of the delicate balance between gravitational and surface tension forces. The higher Bond number implies a stronger gravitational pull, causing the bubble to stretch and deform. However, surface tension acts to minimize the surface area, resisting excessive stretching. The combination of these effects results in the formation of smaller droplets at the periphery, a characteristic feature of peripheral breakup in Regime IV. Fig. 9 illustrates the shape of the pair of bubbles rising in the shear-thinning fluid in regime IV, revealing a peripheral breakup for both the LB and TB at the initial stage of rising before their merging at $t = 5$. Subsequently, the bubbles experience repeated merging and breakup events, giving rise to the formation of larger bubbles and numerous satellites. The unique dynamic behavior of bubbles in regime IV can be distinguished, and a new scenario can be defined as the Coalescence-Breakup (CB) scenario, which is marked by frequent mergings and breakups. The repeated merging and breakup of bubbles create intricate interactions between them, leading to the formation of many satellites. This scenario's behavior is more intricate than the three other scenarios (side escape, DKT, and coalescence). The primary cause of this behavior can be attributed to the high values of Ga and Bo numbers, which result in instability in the dynamics of the bubbles. When the surrounding fluid is shear-thinning, the instability in the bubble dynamics increases due to the reduced viscosity with increasing shear rate. This intricate behavior can be explained by the interplay of various physical factors. The primary drivers of this complex behavior are the elevated values of the Galilei and Bond numbers. In regime IV, where Bond num-

ber is high, the bubble dynamics become susceptible to instability. In the shear-thinning fluid, the reduced viscosity accompanying an increase in shear rate further amplifies this instability by increasing the local Galilei number. The elevated Galilei number indicates a significant influence of inertial forces, promoting dynamic instabilities, while the high Bond number implies substantial gravitational effects. As the bubbles rise, the interplay of these forces leads to peripheral breakup at the initial stage and subsequently results in repeated mergings and breakup events. The Coalescence-Breakup scenario unfolds due to the dynamic competition between the tendency of bubbles to coalesce under gravitational forces and the opposing influence of surface tension, causing breakup. The reduced viscosity in the shear-thinning fluid intensifies these dynamics, giving rise to intricate interactions, frequent mergings, and the formation of numerous satellite bubbles. In essence, the high Ga and Bo numbers, compounded by the shear-thinning nature of the fluid, create a scenario where the delicate balance between gravitational, inertial, and surface tension forces results in the observed Coalescence-Breakup dynamics, setting it apart as a distinctive regime within the broader study of bubble behaviors.

Fig. 10 presents the shape of bubbles rising in the Newtonian fluid in regime IV. In contrast to the shear-thinning case, these bubbles have enough time to coalesce before experiencing any breakup. At $t = 5.05$, the bubbles merge, forming a larger bubble (MB) that subsequently rises vertically. As the MB ascends, its shape transforms into a skirted bubble, indicating a shift in the dynamics behavior from regime IV to regime II. Unlike the bubbles in the shear-thinning case, the bubbles in the Newtonian case follow the coalescence scenario. This behavior is due to the absence of the shear-thinning effect, resulting in a more stable and less complex dynamic pattern. In the case of $n = 1.0$, the local Ga number of the merged bubble is smaller than the initial Ga number, resulting from the reduced rising velocity of the MB compared to the initial bubbles. This decrease in local Ga number leads to the shift in the dynamics behavior of the MB from regime IV to regime II. However, for $n = 0.5$, where the surrounding fluid is shear-thinning, the local Ga number increases, causing the bubbles to break before merging.

In regime V, where both Bond and Galilei numbers are relatively high, the central breakup observed in a single bubble can be attributed to the interplay of buoyancy, surface tension, and fluid dynamics. The central breakup observed in regime V is likely a consequence of the balance between the gravitational forces and the opposing surface tension. Since

Accepted to Phys. Fluids 10.1063/5.0185472

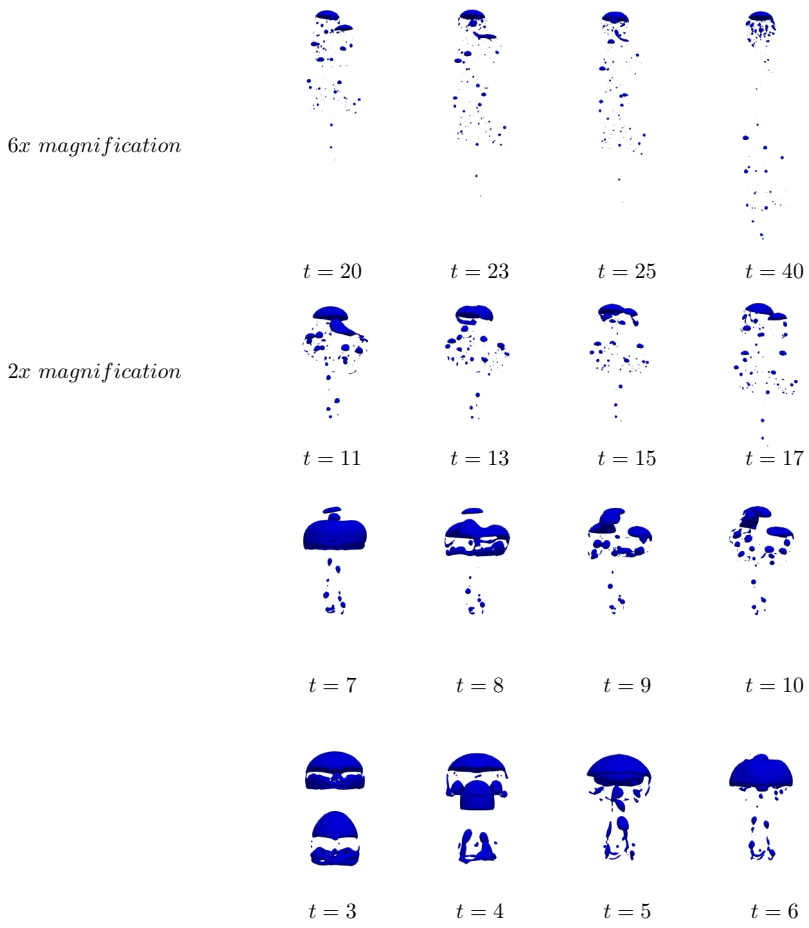

FIG. 9. Shape of the bubbles rising in the shear-thinning fluid ($n = 0.5$, $\lambda = 6$); regime IV with (Ga,Bo)=(30,100).

Bo is relatively high, gravitational forces begin to overpower surface tension, leading to the emergence of intricate patterns in bubble breakup. The balance between buoyancy, gravitational forces, and surface tension in this specific regime leads to a distinctive breakup pattern, characterized by a central rupture rather than peripheral or other types of breakup. Figs. 11 and 12 illustrate the morphology of bubbles in regime V in the shear-thinning fluid

Accepted to Phys. Fluids 10.1063/5.0185472

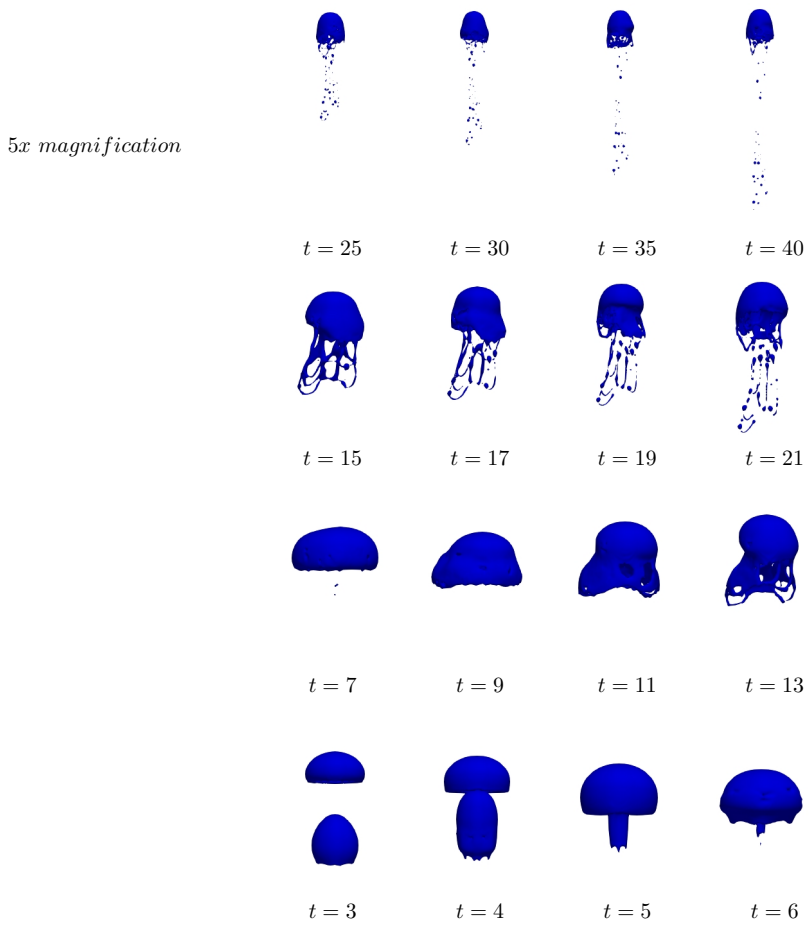

FIG. 10. Shape of the bubbles rising in the Newtonian fluid ($n = 1.0$); regime IV with (Ga,Bo)=(30,100).

and the Newtonian fluid, respectively. In the shear-thinning case, both the LB and TB undergo central breakup initially before any merging occurs. The initial peripheral breakups observed in Newtonian fluids are attributed to the increasing dominance of inertial forces, which overcome the surface tension forces and cause the bubble to rupture at its edges. Subsequently, the bubbles undergo repeated cycles of merging and breaking, leading to the

formation of larger bubbles and numerous satellites. In the Newtonian case, peripheral breakups occur initially for both TB and LB, followed by an initial merging and subsequent central breakup, resulting in the formation of larger bubbles and numerous satellites. The initial peripheral breakups in the Newtonian fluid suggest that surface tension plays a more prominent role, causing rupture at the outer edges of the bubbles. In both cases, the behavior aligns with the CB scenario, where the coalescence and breakup events play a significant role in shaping the dynamics of the bubbles.

In Figs. 9-12, the region of interest for the bubbles dynamically changes over time. This phenomenon is rooted in the temporal evolution of the system, where occurrences such as breakups and the formation of satellites unfold. Notably, these satellites exhibit slower travel velocities compared to the main bubble. Consequently, the region of interest expands as time progresses. It's essential to note that the scaling of the bubbles in these figures deviates from a uniform scale, reflecting the dynamic nature of the evolving phenomena. Magnification indicators have been implemented for enhanced clarity in each case. For instance, in Fig. 9, the cases at $t = 3$ to 10 have been established as the reference magnification. Specifically, for $t = 11 - 17$, a $2x$ magnification has been applied, and for $t = 20 - 40$, a $6x$ magnification has been utilized.

In this comprehensive investigation, the dynamic behavior of the bubble pair across the five different regimes is systematically analyzed, yielding three distinct patterns: 1. Regimes I and III follow either the side-escape scenario or the DKT scenario, exhibiting synchronized rising without any breakup or merging, regardless of the fluid's rheological properties. 2. Regime II displays a coalescence scenario in both the shear-thinning and Newtonian cases, where the bubbles merge without undergoing further fragmentation. 3. Regimes IV and V present a more intricate behavior, involving multiple breakups and mergings, resulting in the formation of satellites and showcasing evident instability.

2. Passive scalar transfer between the bubbles and surrounding fluid

An initially spherical single bubble with an initial concentration of a passive scalar ϕ_0 raises under the action of density-driven buoyancy forces as it displaces the ambient fluid that, in turn, deforms its interface according to the balance between pressure and surface tension forces between the inner and outer fluids. When the ambient fluid has a zero

Accepted to Phys. Fluids 10.1063/5.0185472

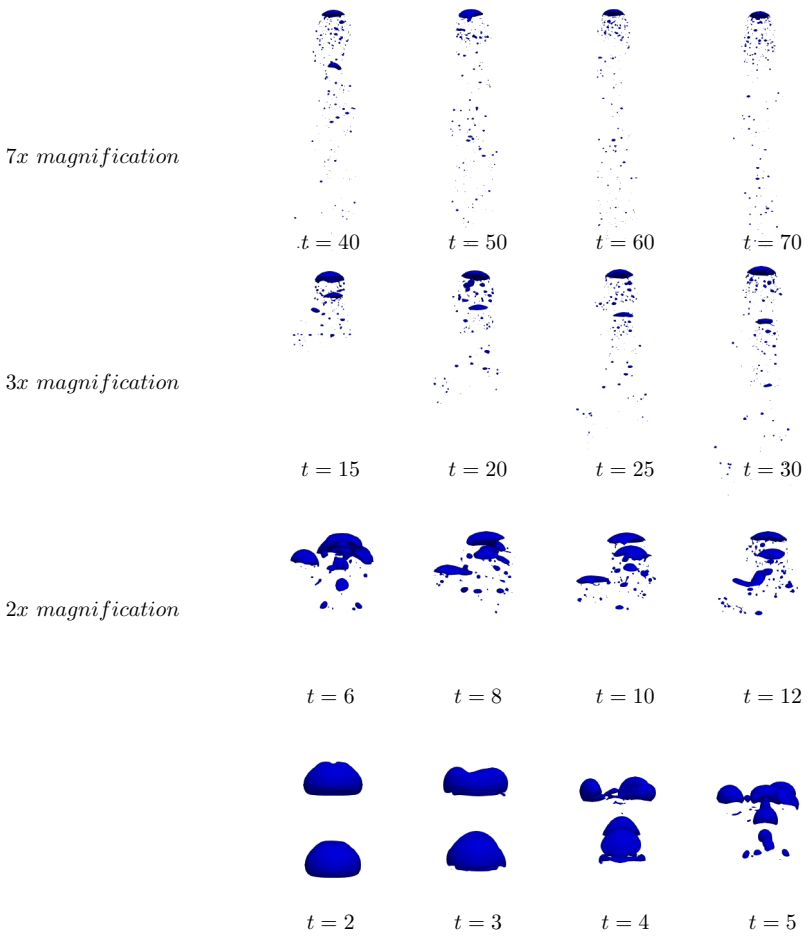

FIG. 11. Shape of the bubbles rising in the shear-thinning fluid ($n = 0.5$, $\lambda = 6$); regime V with (Ga,Bo)=(100,100).

concentration of ϕ, this ascension is accompanied by the exchange of the scalar across the interface. The convective flux of ϕ between the phases depends on the flow hydrodynamics (advection) and the interfacial passive scalar gradient (diffusion).

To quantify the impact of surface tension and rheology on the rate exchange of passive scalar, we computed the surface-average Sherwood number $\langle Sh \rangle$ for each pair of Galilei and

Accepted to Phys. Fluids 10.1063/5.0185472

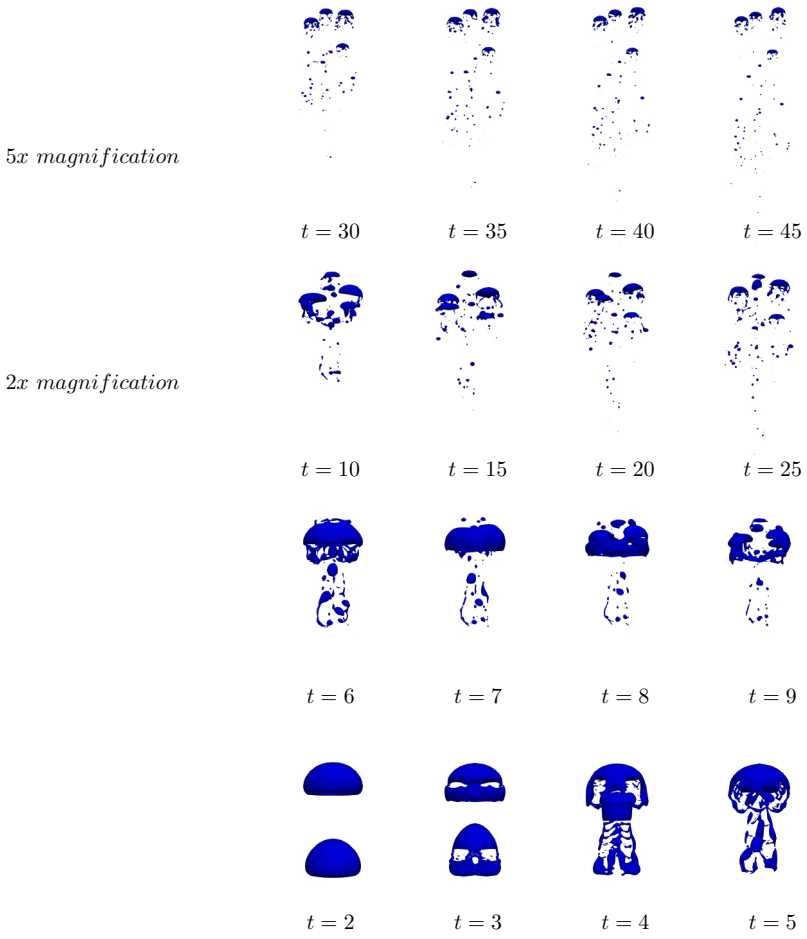

FIG. 12. Shape of the bubbles rising in the Newtonian fluid ($n = 1.0$); regime V with (Ga,Bo)=(100,100).

Bond numbers for each regime discussed before.

In Kazemi et al.[39], the definition of the surface-averaged Sherwood number was introduced as follows (see also their Eq. 19):

$$\langle Sh \rangle = -\frac{\int_V \nabla^2 \phi dV}{\phi_{\text{ref}}} = \frac{q_\phi}{\phi_{\text{ref}}} \tag{8}$$

where q_ϕ is the non-dimensional time evolving surface averaged scalar mass transfer rate and ϕ_{ref} is the non-dimensional reference concentration. According to Kazemi et al.[39], ϕ_{ref} is defined as the non-dimensional time-evolving surface-averaged value of the scalar, $\langle \phi_s \rangle$, at the bubble interface. This definition yields a quasi-steady Sherwood number, enabling the characterization of mass transfer efficiency at each time step. This definition contributes to the development of an empirical correlation between the Sherwood number and the Peclet number within a quasi-steady context, $\langle Sh \rangle \approx Pe^{\alpha}$.

Nevertheless, for the analysis of the temporal evolution of scalar flux, it is more suitable to set ϕ_{ref} as the value of ϕ_0 at the initial time.

By adopting this alternative definition, we can derive a transient Sherwood number, Sh_t, that explicitly portrays the scalar flux as a transient process:

$$Sh_t = \frac{q_\phi}{\phi_0} \tag{9}$$

This, in turn, allows for the computation of a scaling law between Sh_t and time within a transient scenario, $Sh_t \approx t^{\beta}$.

Figure 13 illustrates the surface-averaged Sherwood number for the leading bubble (black) and the trailing bubble (red) rising in both shear-thinning (solid lines) and Newtonian (dashed lines) fluids within regime I. Additionally, the figure includes the surface-averaged Sherwood number evolution for a single bubble ascending in shear-thinning and Newtonian fluids, depicted by solid and dashed blue lines, respectively, for comparison.

Following an initial rapid decline in the surface-averaged Sherwood number, the LB exhibits a surface-averaged Sherwood number similar to that of a single bubble, irrespective of the fluid's rheological properties. In contrast, the TB's surface-averaged Sherwood number is lower while it trails the LB during the drafting stage. As the TB moves away from the LB's wake in scenarios like side escape or DKT and the pair transitions into a side-by-side arrangement, the TB's surface-averaged Sherwood number increases until it reaches a quasi-terminal value comparable to that of the LB.

The consistently higher surface-averaged Sherwood number in the shear-thinning case can be attributed to a more rapid shift from being in line with the TB under the LB's wake effect to adopting a side-by-side configuration. This results in an increased interfacial area between the bubbles and the surrounding fluid without the influence of the wake. This enlarged interfacial area, devoid of wake effects, leads to higher mass transfer rates and,

consequently, a higher surface-averaged Sherwood number.

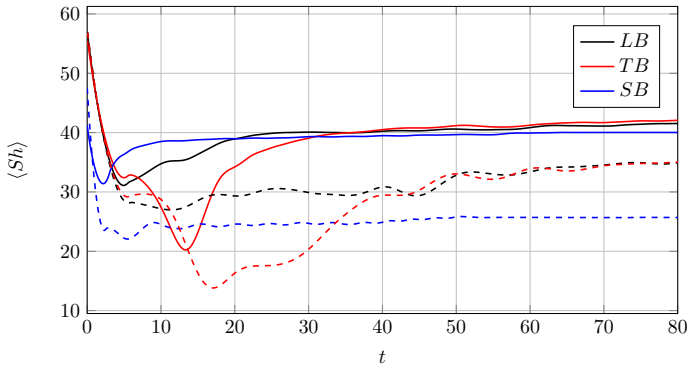

FIG. 13. Evolution of surface-averaged Sherwood number for a pair of bubbles (black and red) and a single bubble (blue) rising in regime I with (Ga,Bo)=(10,1). Solid lines: shear-thinning case ($n = 0.5$, $\lambda = 6$), and dashed lines: Newtonian case.

Fig. 14 provides a comprehensive analysis of the instantaneous vertical distance between the bubbles, rising velocity magnitude of the bubbles, and transient Sherwood number for both the pair of bubbles and a single bubble ascending in regime I (left) and regime III (right). Similarly, Fig. 15 presents the corresponding data for regime II. Additionally, Fig. 16 displays the rising velocity magnitude of the bubbles and transient Sherwood number for both the pair of bubbles and a single bubble ascending in regime IV (left) and regime V (right). In all three figures, the solid lines represent the shear-thinning case, while the dashed lines represent the Newtonian case.

Accepted to Phys. Fluids 10.1063/5.0185472

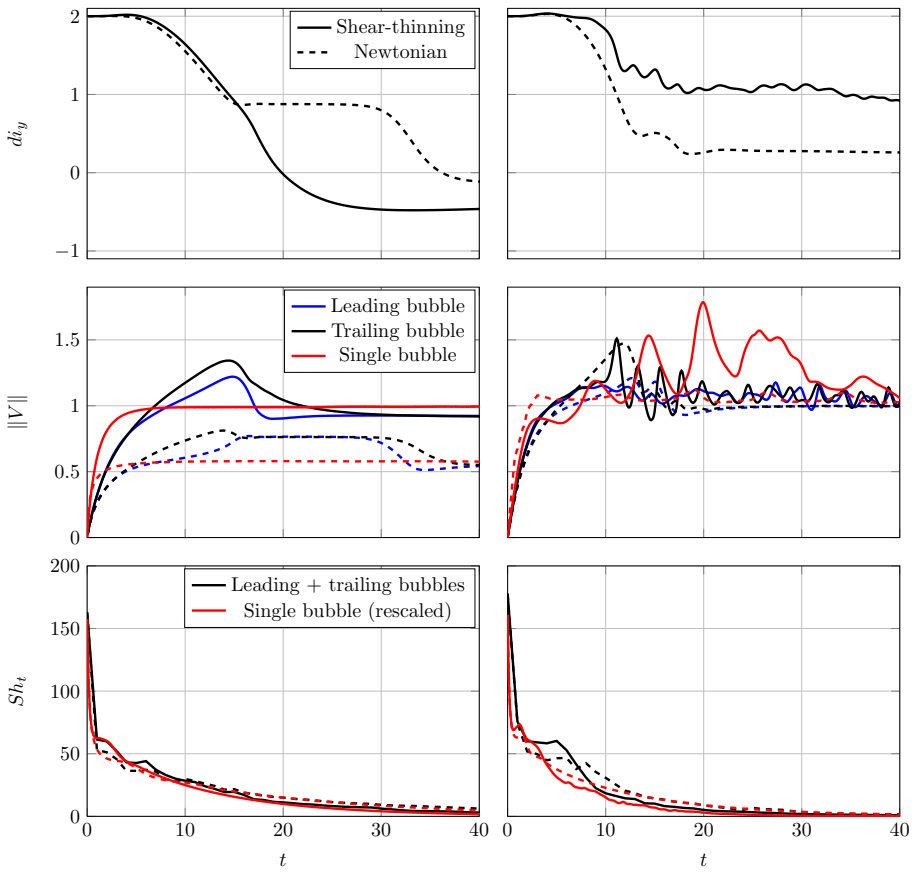

FIG. 14. Evolution of instantaneous vertical distance between the bubbles, rising velocity magnitude of the bubbles, and transient Sherwood number. Left: regime I with (Ga,Bo)=(10,1), and right: regime III with (Ga,Bo)=(50,2). Solid lines: shear-thinning case, and dashed lines: Newtonian case.

Accepted to Phys. Fluids 10.1063/5.0185472

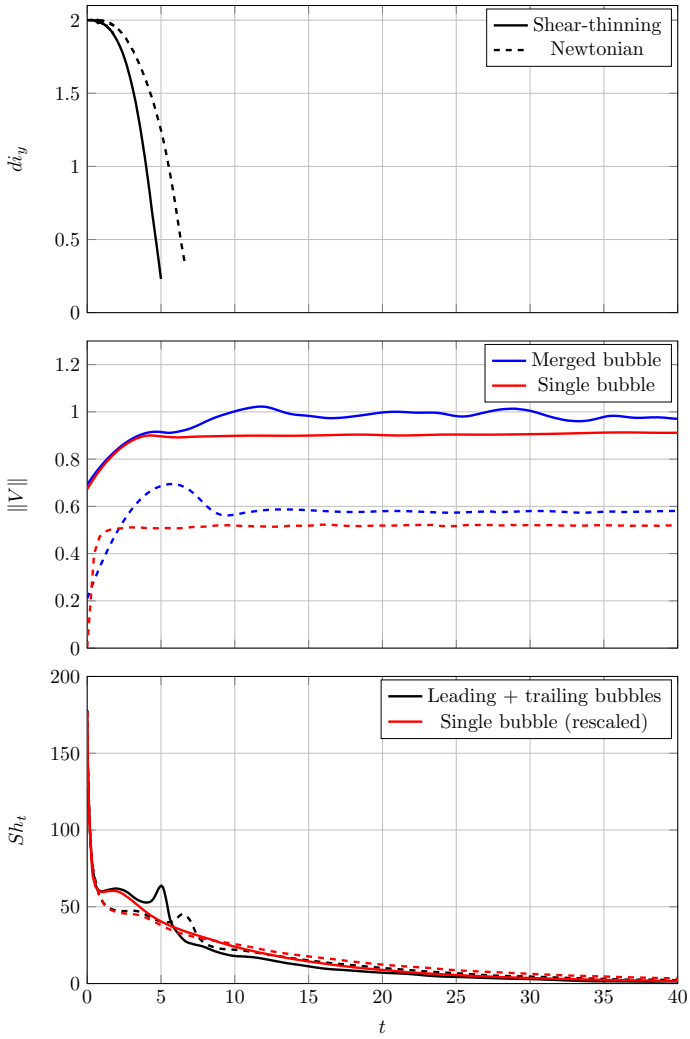

FIG. 15. Evolution of instantaneous vertical distance between the bubbles, rising velocity magnitude of the bubbles, and transient Sherwood number in regime II with (Ga,Bo)=(10,100). Solid lines: shear-thinning case, and dashed lines: Newtonian case.

Given that all simulations commence with the same initial value of ϕ, the area under all curves, i.e.,

$$\frac{1}{Pe_B\, V}\int_0^\infty Sh_t dt = \phi_0, \tag{10}$$

remains consistent and equals the initial total amount of passive scalar within the bubble.

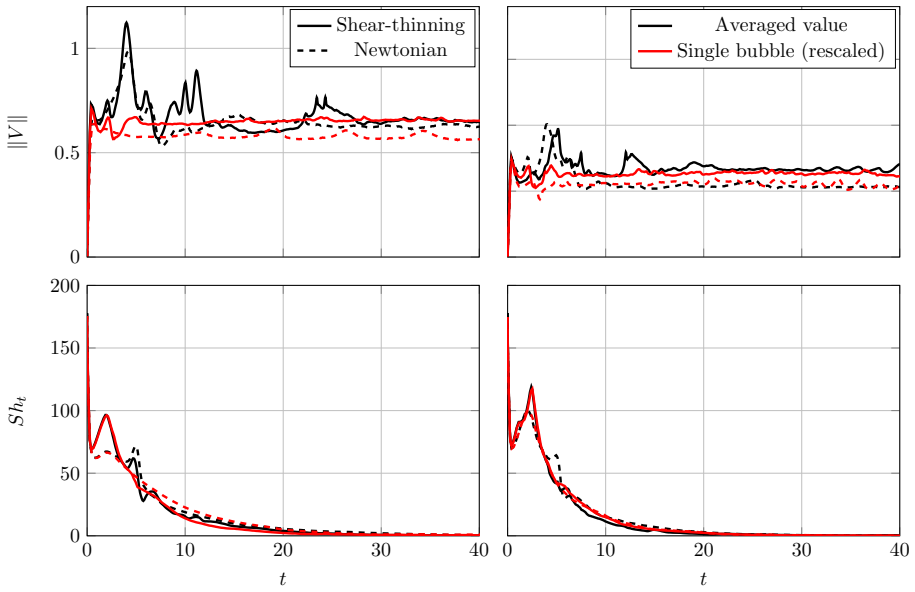

FIG. 16. Evolution of rising velocity magnitude of the bubbles and transient Sherwood number. Left: regime IV with (Ga,Bo)=(30,100), and right: regime V with (Ga,Bo)=(100,100). Solid lines: shear-thinning case, and dashed lines: Newtonian case.

Furthermore, it is essential to note that since the initial surface area for the pair of bubbles is twice that of a single bubble, a rescaled Sh_t is reported for a single bubble, which is then multiplied by two. This consideration ensures an accurate comparison between the pair of bubbles and a single bubble during the analysis.

For a single bubble, the findings reveal an initial rapid decrease in the interfacial exchange rate of ϕ, represented by Sh_t, as the concentrations of the passive scalar on both sides of the interface become equal. Notably, regimes IV and V exhibit the highest flux rate of the passive scalar, suggesting that the increase in interface surface due to break-up enhances transport. In contrast to regimes I and II, characterized by a monotonically decreasing Sh_t,

regimes III to V, with an increasing number of daughter bubbles, display a local maximum of growing magnitude.

Furthermore, by definition, the integral of the difference between the transient Sherwood number of the Newtonian case, $Sh_{t_{\mathrm{N}}}$, and the shear thinning case, $Sh_{t_{\mathrm{ST}}}$, tends to zero as time approaches infinity. Generally, in the shear-thinning case, the reduction in viscosity around the bubble leads to an initially faster exchange rate of the passive scalar, which eventually becomes slower compared to the Newtonian case.

For an in-line pair of bubbles, the trailing bubble initially remains within the wake of the leading bubble, which is enriched with ϕ. Subsequently, the pair may diverge laterally from each other (regimes I and III), merge into a larger single bubble (regime II and regime IV in the Newtonian case), or rapidly break apart (regime IV in the shear-thinning case and regime V). Similar to the behavior observed for a single bubble, regimes IV and V demonstrate the most rapid transfer of passive scalar during the early stages of ascent due to multiple break-up events that rapidly increase the interface area.

Furthermore, in the comparison between both rheologies, the shear-thinning case exhibits a generally faster passive scalar exchange initially, compared to the Newtonian case. As the regime transitions from I to V, the pair of bubbles display more intricate dynamics characterized by oscillatory trajectories and breakup events, resulting in progressively larger fluctuations of Sh_t during the early stages of ascent, which inevitably diminish as the amount of ϕ within the bubble decreases.

When comparing a single bubble with a pair of bubbles, in the Newtonian case, a transient stage with a higher normalized exchange rate for the pair of bubbles compared to a single bubble is observed, specifically in Regimes I and III, where the pair of bubbles align side-by-side. However, only Regime II shows an improved, quasi-terminal value of transport efficiency for the single bubble. In the shear-thinning case, the presence of a second bubble enhances the passive scalar exchange rate in Regimes I and III, which are characterized by a side-by-side terminal arrangement of the pair of bubbles. Additionally, Regime IV also exhibits a larger normalized exchange rate than that for a single bubble. However, the normalized exchange efficiency in Regime II is hindered by the early merging of the pair of bubbles. Similarly, in Regime V, characterized by the rapid breakup of the bubbles, which significantly enhances the transport of ϕ, the single bubble case also exhibits a larger normalized exchange rate.

Noticeably, specific plots depicting the transient Sherwood number over time reveal distinct oscillations. These fluctuations, well-documented as a characteristic of mass transfer within a fluid sphere in prior studies[45,46], are a consequence of the existence of an internal Hill's vortex[47]. These vortices maintain a continuous supply of fresh and enriched fluid from the bubble's core to its interface. The intensity of this internal vortex is controlled by the alignment of velocity and the shear stress of viscosity at the interface.

B. Effects of the bubble pair radius ratio R_r

In the context of bubbly flows, bubbles often exhibit different sizes. In this section, the influence of bubble size on both bubble interactions and mass transfer rates is explored. The bubble pair radius ratio, denoted as R_r, is defined as the ratio of the leading bubble's radius (R_{LB}) to the trailing bubble's radius (R_{TB}). Specifically, the focus is on the case of $Ga = 50$ and $Bo = 2$, corresponding to regime III. Three distinct bubble pair radius ratios are investigated: 2, 1, and 0.5, with $Ga = 50$ and $Bo = 2$ being based on the smaller bubble in each case.

Fig. 17 presents the shapes of bubbles ascending in the shear-thinning fluid ($n = 0.5$, $\lambda = 6$) with varying bubble pair radius ratios (R_r). When $R_r = 0.5$, meaning the trailing bubble (TB) has a larger radius than the leading bubble (LB), a fascinating interplay occurs. The sheltering effect, which usually facilitates merging, is not strong enough to induce immediate coalescence. However, it still plays a crucial role by increasing the local Galilei and Bond numbers of TB. These elevated Ga and Bo numbers lead to significant deformations and instability in TB's trajectory, eventually culminating in its breakup around $t = 17$. The resulting three bubbles then ascend in a zigzag pattern, characteristic of regime III. This zigzag behavior is indicative of lateral oscillations, often associated with the interaction of bubbles in shear-thinning fluids. The sheltering effect, while not directly causing immediate merging, introduces complexities that contribute to the unique trajectory observed post-breakup. The influence of Ga and Bo numbers on the ensuing dynamics underscores the nuanced interplay of forces in shear-thinning conditions. This scenario showcases how the sheltering effect, although not causing immediate merging, can substantially influence the local dynamics and lead to breakup due to increased Ga and Bo.

Conversely, for $R_r = 2$, where the trailing bubble has a smaller radius, the sheltering

effect of the larger leading bubble becomes particularly influential. At $t = 3$, the bubbles come into contact, and due to the substantial sheltering, TB is rapidly engulfed by LB. This rapid coalescence results in the formation of a merged bubble (MB). The sheltering effect is a consequence of the interaction between LB and TB, where LB shields TB from the surrounding fluid, creating conditions conducive to quick merging. The merged bubble exhibits a Galilei number of approximately 70 and a Bond number of about 5. These values align with conditions characteristic of regime III, as previously depicted in Fig. 6. These values suggest that, despite the rapid merging, the resulting MB still experiences gravitational forces that contribute to its distinctive behavior. Post-merging, the MB continues its ascent in a spiral trajectory. This spiral motion indicates a complex interplay of forces, including gravitational and viscous forces, as well as the effects of shear-thinning on viscosity. The substantial deformations observed in the spiral trajectory highlight the dynamic nature of the bubble in shear-thinning conditions. The influence of the initial geometric configuration, along with the inherent characteristics of shear-thinning fluids, contributes to the nuanced behavior observed during the ascent of the merged bubble. The behavior of the bubbles with $R_r = 1$ has been previously discussed in the preceding subsection.

Fig. 18 shows the shapes of bubbles ascending in the Newtonian fluid ($n = 1.0$) with different R_r values. When $R_r = 0.5$, the sheltering effect of the leading bubble is not potent enough to induce significant interaction or merging between the bubbles. Consequently, both LB and TB continue to rise vertically while maintaining their initial separation. Despite undergoing some deformation, TB in the Newtonian fluid does not undergo breakup, contrasting with its counterpart in the shear-thinning fluid. The lower local Galilei number for TB in the Newtonian fluid contributes to reduced deformations and a lower likelihood of breakup compared to the shear-thinning case. The observed behavior in the Newtonian fluid contrasts with the corresponding case in the shear-thinning fluid. In the shear-thinning fluid, the reduced viscosity around TB due to shear-thinning effects could contribute to a more dynamic interaction with LB, leading to breakup. However, in the Newtonian fluid, the lower local Ga values for TB result in a more stable ascent without breakup. The behavior of the bubbles in the Newtonian fluid emphasizes the influence of fluid properties, specifically the absence of shear-thinning effects. Without the variations in viscosity associated with shear-thinning, the dynamics are primarily governed by gravitational and viscous forces. The bubbles maintain a more straightforward vertical ascent, highlighting the importance

Accepted to Phys. Fluids 10.1063/5.0185472

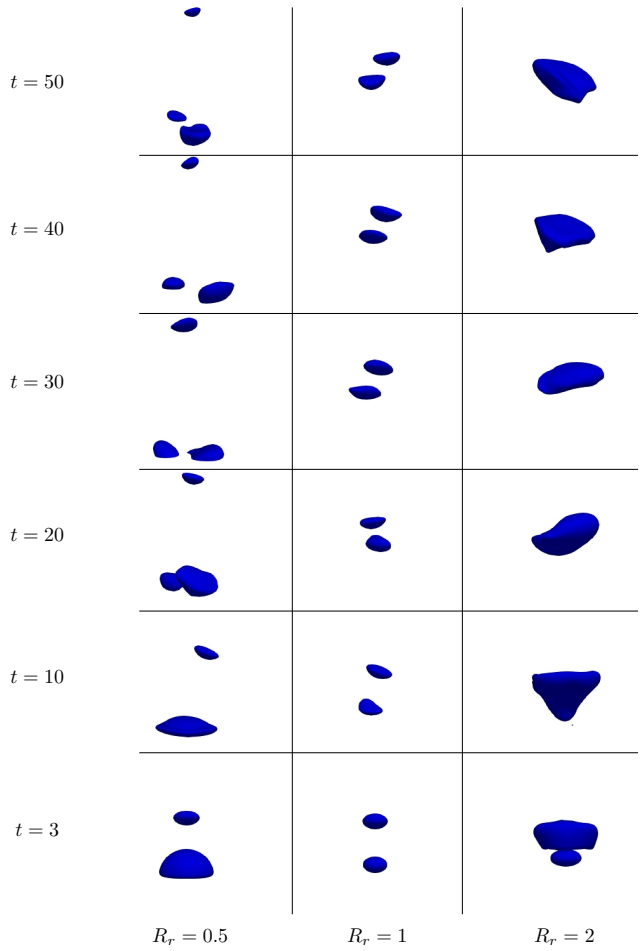

FIG. 17. Shape of the bubbles rising in the shear-thinning fluid ($n = 0.5$, $\lambda = 6$) for different R_r; regime III with (Ga,Bo)=(50,2).

of considering fluid rheology in understanding bubble dynamics.

In contrast, when $R_r = 2$, the sheltering effect of the leading bubble becomes more pronounced. The larger LB accelerates the rise of TB as they come into contact, leading to a merger. The sheltering effect refers to the influence of the larger bubble on the motion of the smaller one, and in this case, it results in a more rapid ascent of TB. The accelerated

rise due to the sheltering effect culminates in the merging of TB with LB, forming a merged bubble (MB). This merging event is a consequence of the dynamics of the two bubbles interacting in a way that leads to their coalescence. The specific conditions in this scenario, including the radius ratio between the bubbles, create an environment where the sheltering effect plays a decisive role in inducing merging. In the Newtonian fluid, the merged bubble (MB) experiences fewer deformations compared to the case of shear-thinning fluid. In the shear-thinning case, the reduced viscosity around the trailing bubble due to shear-thinning effects could contribute to more substantial deformations and a different dynamic interaction with the leading bubble. In the Newtonian fluid, the sheltering effect and the influence of fluid properties, especially viscosity, result in the formation of a merged bubble with less pronounced deformations. The behavior of the bubbles with $R_r = 1$ has been discussed in the previous subsection.

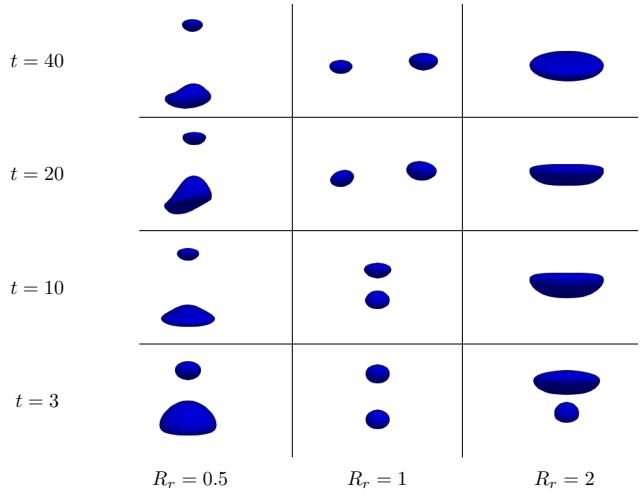

FIG. 18. Shape of the bubbles rising in the Newtonian fluid ($n = 1.0$) for different R_r; regime III with (Ga,Bo)=(50,2).

Fig. 19 presents the instantaneous vertical distance between the bubbles and the rising velocity magnitude of the bubbles for different values of R_r. In the Newtonian case, the velocity magnitude exhibits an oscillatory behavior for $R_r = 0.5$, indicating a zigzag path during the bubble's ascent. In contrast, the oscillations are less pronounced for $R_r = 2$, and

the merged bubble (MB) rises in a spiral path with a smaller domain. The rising velocities for $R_r = 0.5$ and $R_r = 1$ are comparable, while the MB for $R_r = 2$ rises slightly faster due to its larger radius, resulting in a higher local Ga.

Similarly, in the shear-thinning case, the magnitude of the rising velocity of the MB ($R_r = 2$) is greater than that of the other cases. The higher magnitude of the MB's rising velocity for $R_r = 2$ is attributed to the sheltering effect induced by LB, causing TB to merge with LB, resulting in a larger bubble with a higher rising velocity. This effect is also observed in the shear-thinning case, where MB exhibits the highest rising velocity magnitude. However, the oscillatory behavior observed in the shear-thinning case is less pronounced in the Newtonian case due to the constant viscosity of the fluid.

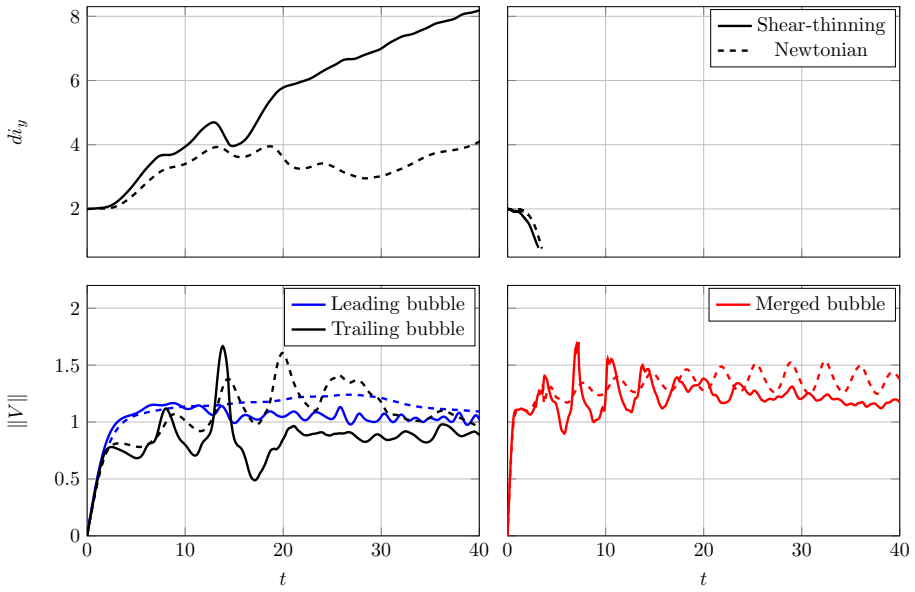

FIG. 19. Evolution of instantaneous vertical distance between the bubbles and rising velocity magnitude of the bubbles. Left: $R_r = 0.5$, and right: $R_r = 2$. Solid lines: shear-thinning case, and dashed lines: Newtonian case; regime III with (Ga,Bo)=(50,2).

The transient Sherwood number evolution for different R_r values is depicted in Fig. 20. It is important to mention that the reported Sh_t includes the combined Sherwood numbers of both LB and TB. Moreover, for the $R_r = 1$ case, the reported Sh_t is scaled by a factor of

2.5 to account for the smaller initial surface area of the bubbles compared to the other two cases, which is 2.5 times smaller. The analysis of the data reveals that when the two bubbles have equal radii, the exchange efficiency is relatively slower in the initial stages compared to other scenarios. This might be attributed to the fact that the two bubbles are of the same size, leading to less efficient transport of passive scalar at the interface between them. As the bubble radius ratio increases, the exchange efficiency is hindered by the early merging of the pair of bubbles. Generally, in the shear-thinning scenario, the reduced viscosity around the bubble results in a faster initial exchange rate of the passive scalar. However, over time, this rate diminishes and becomes slower compared to the Newtonian case.

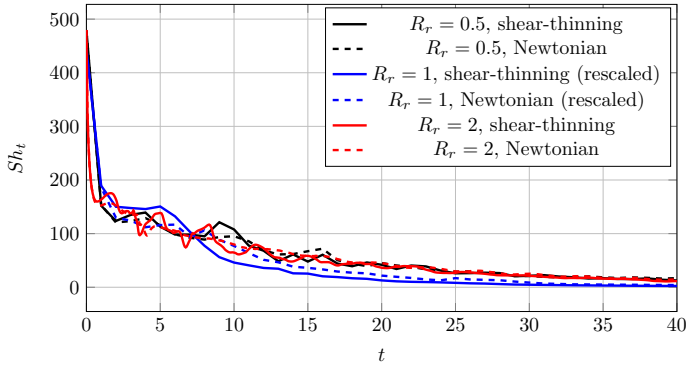

FIG. 20. Evolution of transient Sherwood number for different values of R_r for both the shear-thinning and Newtonian cases; regime III with (Ga,Bo)=(50,2).

C. Effects of the inelastic time constant λ

In the Carreau model for the viscosity field of non-Newtonian fluids, the inelastic time constant is an important parameter that affects the rheological behavior of the fluid. Zero inelastic time constant means that the fluid is Newtonian while for large values of λ, the Carreau model reduced to power-law model[48]. To explore the impact of λ on both bubble dynamics and mass transfer rates, we have chosen a specific set of conditions denoted as (Ga, Bo)=(50,2), situating us within regime III of the $Ga - Bo$ phase diagram. Within this regime, we have investigated four distinct values of λ: 0 (representing a Newtonian fluid), 3, 6, and 9.

Fig. 21 illustrates the progression of bubble shapes under varying λ values. As previously discussed, the dynamic characteristics of the λ=0 case have been detailed in earlier sections. In this instance, the behavior aligns with the DKT scenario, with bubbles persistently ascending in a vertical, side-by-side manner following an initial transient phase. Conversely, for the other three cases (λ=3, 6, and 9), the bubbles adopt an alternative path recognized as the side escape scenario. Initially, the rising velocity of TB increases due to the sheltering effect caused by LB. Subsequently, TB manages to escape from the wake of LB, ultimately continuing its ascent characterized by a distinctive zigzag pattern.

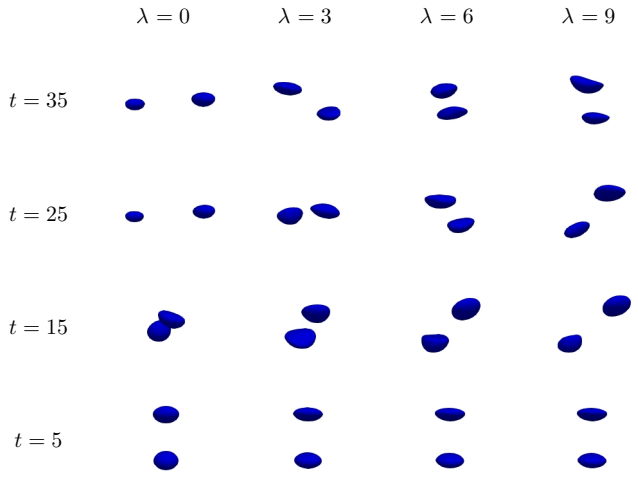

FIG. 21. Shape of the bubbles for different values of λ at different times; regime III with (Ga,Bo)=(50,2).

Fig. 22 displays several key parameters, including the instantaneous vertical separation between the bubbles, the magnitude of the rising velocity for both the leading bubble ($\|V\|_{LB}$) and trailing bubble ($\|V\|_{TB}$), as well as the transient Sherwood number. It's notable that with an increase in λ, the oscillatory behavior of the bubbles becomes more pronounced. This heightened oscillation is also clearly evident in the rising velocity magnitude. Nonetheless, it is noticeable that in all three cases exhibiting shear-thinning behavior, the rising velocity magnitude demonstrates periodic fluctuations around a consistent value. This constant value closely approximates the magnitude of the rising velocity observed when

Accepted to Phys. Fluids 10.1063/5.0185472

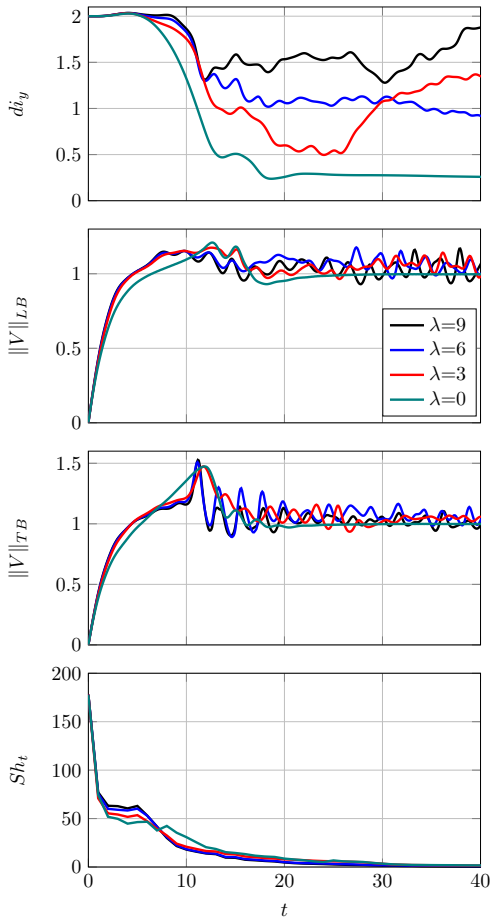

FIG. 22. Evolution of instantaneous vertical distance between the bubbles, rising velocity magnitude of LB ($\|V\|_{LB}$), rising velocity magnitude of TB ($\|V\|_{TB}$), and transient Sherwood number in regime III with (Ga,Bo)=(50,2).

λ=0. Furthermore, we observe that the initial rate of passive scalar exchange is more rapid for smaller λ values, gradually slowing down in comparison to cases with higher λ values. To gain further insight into these dynamics, we conducted a fast Fourier transform (FFT) of the rising velocity magnitude over time, revealing the primary frequencies for λ=3, 6, and 9 as 0.4, 0.44, and 0.48, respectively.

D. Effects of the flow index n

The flow index indicates the degree of non-Newtonian characteristics of the fluid. As a fluid becomes more shear thinning, n decreases while for Newtonian fluids it is equal to 1. To study the effects of the flow index, we have used the parameters taken from Cano-Lozano and Martínez-Bazán[32] (Bubble25) as the following: $Ga = 88.74$ and $Bo = 8.5$ (regime III), with four different flow indexes: n =0.3, 0.5, 0.7, and 1.0 with $\lambda = 6$.

Fig. 23 illustrates the evolution of bubble shapes within fluids characterized by different values of n. As observed, there is a distinct alteration in bubble morphology associated with changes in the n parameter. In the context of shear-thinning fluids with $n < 1$, the bubbles ascend following a zigzag trajectory, indicative of the presence of shear-thinning and viscoelastic influences that result in substantial bubble deformation. When n increases within shear-thinning fluids (n =0.3, 0.5, and 0.7), the extent of this zigzag path diminishes. This behavior finds its origin in the fluid's viscosity characteristics. Shear-thinning fluids exhibit intricate rheological properties, where viscosity adjusts with changes in shear rate. Consequently, as bubbles rise in such fluids, they generate a flow field that alters the local shear rate, contributing to complex and erratic bubble motion. Hence, a reduction in n corresponds to an expanded domain of the zigzag path, signifying a more pronounced impact of the fluid's rheology on the bubble's trajectory. Furthermore, it is evident that a reduction in the flow index leads to an earlier occurrence of bubble merging.

In contrast, for Newtonian fluids characterized by $n = 1$, the bubbles initially follow a zigzag course. However, as they continue to ascend, the domain of this zigzag path diminishes, eventually transitioning into a vertical trajectory. This phenomenon is rationalized by the fact that the vertical path minimizes drag force, offering the lowest drag coefficient. Consequently, the bubbles strive to adopt this path to mitigate the drag force acting upon them.

The progression of the rising velocity magnitude of the bubbles and the transient Sherwood number is displayed in Fig. 24 across varying values of n. It is observable that in the case of Newtonian fluid ($n = 1$), the bubbles initially exhibit fluctuating velocities. However, as the bubbles ascend, these fluctuations gradually subside, leading to a nearly constant velocity. This transition is a result of the dominating influence of fluid viscosity over other fluid-related effects.

Accepted to Phys. Fluids 10.1063/5.0185472

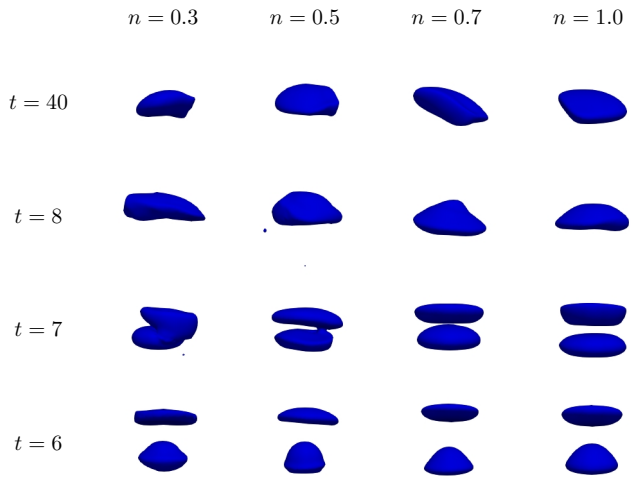

FIG. 23. Shape of the bubbles for different values of n with $\lambda = 6$ at different times; regime III with (Ga,Bo)=(88.74,8.5).

Conversely, in shear-thinning fluids characterized by $n = 0.3$, 0.5, and 0.7, the bubbles consistently maintain an oscillatory pattern in their rising velocity magnitude. This persistence underscores the continued impact of non-Newtonian effects on the trajectory of the bubbles. This oscillatory behavior is also mirrored in the transient Sherwood number, although it is worth noting that the influence of n on Sh_t is relatively small in these cases.

E. Scaling laws for Sherwood number

Fig. 25 illustrates the correlation between the surface-averaged Sherwood number and the Peclet number. In this representation, the blue line corresponds to experimental data sourced from Roudet et al.[49], the red line depicts simulations of a single bubble in a Newtonian fluid, as found in Kazemi et al.[39], and the green line reflects simulations of a single bubble in a shear-thinning fluid, also derived from Kazemi et al.[39]. Additionally, data points on the graph indicate the behavior of leading and trailing bubbles in regimes I and III.

Accepted to Phys. Fluids 10.1063/5.0185472

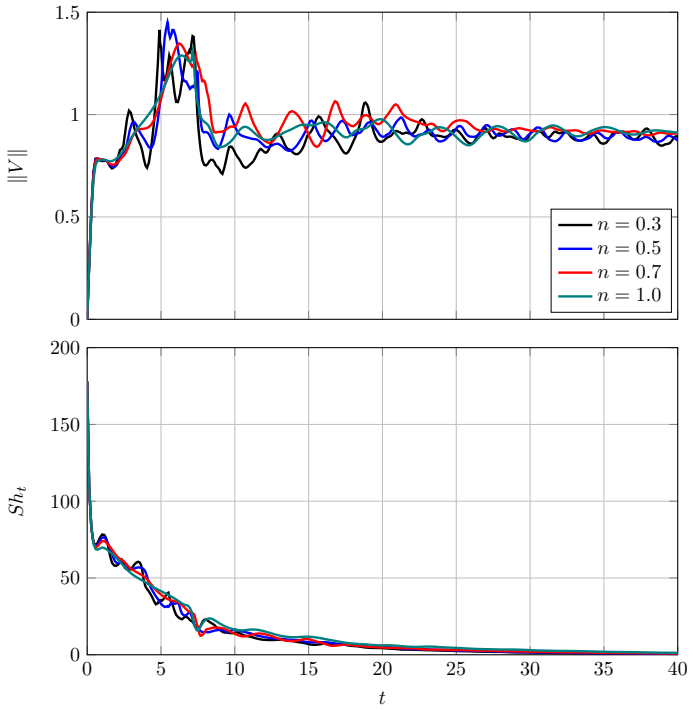

FIG. 24. The evolution of rising velocity magnitude of the bubbles and transient Sherwood number for different values of n with $\lambda = 6$; regime III with (Ga,Bo)=(88.74,8.5).

Accepted to Phys. Fluids 10.1063/5.0185472

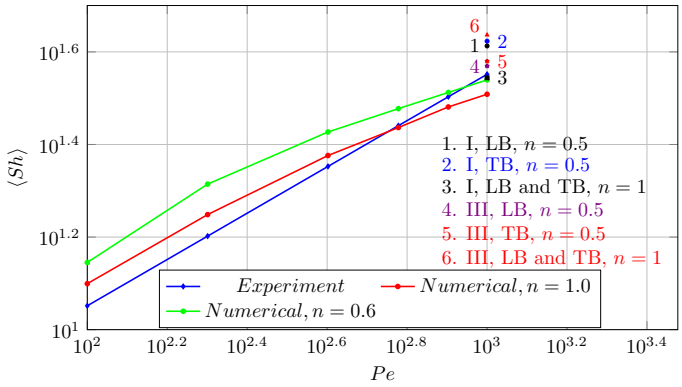

FIG. 25. The logarithmic relationship between the surface-averaged Sherwood number and the Peclet number. The blue line represents experimental data from Roudet et al.[49], the red line represents simulations of a single bubble in a Newtonian fluid[39], and the green line represents simulations of a single bubble in a shear-thinning fluid[39]. Data points on the graph correspond to the leading and trailing bubbles in regimes I and III.

Notably, in regimes I and III, where the bubbles undergo side escape or DKT scenarios, the surface-averaged Sherwood number closely aligns with experimental values for a single bubble. When we apply the quasi-steady definition of the surface-averaged Sherwood number, it becomes apparent that $\langle Sh \rangle$ exhibits a proportional relationship to Pe raised to the power of c_1. Specifically, c_1 assumes a value of 0.5 for a single bubble rising in a Newtonian fluid and 0.46 for a single bubble in a shear-thinning fluid. This correlation can be broadened to account for the influence of multiple parameters, including n, Bo, and Ga, as indicated by the following expression: $\langle Sh \rangle \approx Pe^{c_1}$.

In Fig. 26, the logarithmic progression of the transient Sherwood number for both a single bubble and a pair of bubbles (referred to as LB and TB) ascending in a shear-thinning fluid with specified parameters ($n = 0.5$, $\lambda = 6$) is illustrated. This analysis pertains to regime I with characteristic dimensionless numbers (Ga,Bo)=(10,1).

Accepted to Phys. Fluids 10.1063/5.0185472

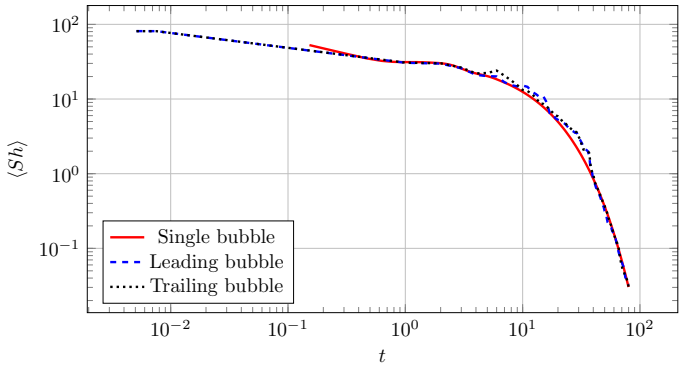

FIG. 26. The logarithmic evolution of the transient Sherwood number for a single bubble and a pair of bubbles rising in the shear-thinning fluid ($n = 0.5$, $\lambda = 6$); regime I with (Ga,Bo)=(10,1).

It is evident that the transient Sherwood number exhibits a proportionality to time raised to the power of c_2. In the context of Fig. 26, it becomes evident that during the initial period, $t < 10$, the exponent c_2 exhibits values of approximately -0.34, -0.36, and -0.28 for the single bubble, LB, and TB, respectively. As time progresses beyond $t > 10$, these values undergo a significant shift, converging to approximately -2.8, -2.96, and -2.94 for the single bubble, LB, and TB, respectively. Notably, the transient Sherwood numbers of LB and TB remain quite similar, with a noticeable difference occurring within the time interval of approximately $6 < t < 16$, where TB approaches LB before ultimately escaping from its wake.

This correlation can be extended to encompass the influence of various parameters such as n, Bo, and Ga through the following expression: $Sh_t \approx t^{c_2}$

VI. CONCLUSIONS

This research embarked on a meticulous exploration of the behavior of a pair of in-line rising bubbles in diverse fluid environments, ranging from Newtonian to shear-thinning fluids. We delved into the intricate interplay of multiple parameters, including Galilei and Bond numbers (Ga and Bo), bubble pair radius ratios (R_r), the inelastic time constant (λ), and the flow index (n). In particular, our exploration ventured into both the realm of hydrodynamics and passive scalar transport, unraveling remarkable patterns and behaviors.

To this end, we used the CFD code *Basilisk* that implements the VOF method with adaptive mesh refinement. Here are the key findings:

In the realm of hydrodynamics, our examination of Galilei and Bond numbers (Ga and Bo) unveiled five distinct regimes that encapsulate the diverse behaviors of single spherical bubbles. These regimes acted as the backdrop against which the interactions of two bubbles, as they traversed this phase space together, played out. From the coalescence of bubbles to the side escapes and the Drafting-Kissing-Tumbling (DKT) phenomena, the role of initial conditions and fluid properties became undeniable. We also defined a new scenario that exhibits the dynamics of a pair of bubbles called the coalescence-breakup scenario. We delved even deeper by exploring the effects of the bubble pair radius ratio (R_r), revealing that this parameter profoundly influences the interactions between bubbles. Smaller R_r values induced pronounced deformations and eventual breakups, while larger R_r values facilitated merging, leading to intriguing variations in rising velocities and passive scalar transfer. Our study further extended to the investigation of λ and n. We revealed that λ played a pivotal role in shaping bubble dynamics. High λ values triggered more pronounced oscillations in bubble behavior, shedding light on the intricate dynamics within these complex fluids. The exploration of n revealed intriguing bubble trajectories. Smaller n values caused more pronounced zigzag paths and earlier bubble merging. In contrast, the highest n value (Newtonian fluid) resulted in bubbles transitioning to a vertical path.

In the realm of passive scalar transfer between the bubbles and the surrounding fluid, we departed from conventional assumptions of constant interface concentration, instead embracing the transient nature of scalar exchange. This nuanced perspective uncovered a wealth of information. Across the varied parameters and scenarios, we observed intriguing trends. In shear-thinning fluids, the initial rate of passive scalar transfer was generally swift due to the reduced viscosity around the bubbles. However, this rate gradually converged with that of Newtonian fluids over time, revealing the temporal intricacies of scalar exchange. Additionally, we conducted detailed analyses comparing the exchange efficiency between single bubbles and pairs of bubbles. This comparison revealed that the presence of a second bubble in a pair often enhanced the passive scalar exchange rate, particularly when the bubbles adopted side-by-side trajectories.

In summary, our comprehensive study has not only enriched our understanding of bubble dynamics in diverse fluid environments but has also unearthed critical insights into passive

scalar transport. This newfound knowledge carries implications across a spectrum of disciplines, from chemical engineering to environmental sciences, with the potential to drive innovation and progress in these fields. As we continue to unlock the mysteries of these intricate systems, we set the stage for further discoveries and advancements in fluid dynamics.

VII. ACKNOWLEDGEMENTS

This work was funded by the Spanish Ministerio de Ciencia, Innovación y Universidades through the grants RTI2018-100907-A-I00 (MCIU/AEI/FEDER, UE), DPI2016-75791-C2-1-P, and PID2020-113303 GB-C21, and also by the Generalitat de Catalunya through the grant 2021-SGR-00732. I also would like to thank the HPC-Europa3 Programme for the received grant that allowed me to visit the ZARM research group at the University of Bremen (Germany) and especially to Prof. Marc Ávila for his guidance and support during my stay.

DATA AVAILABILITY STATEMENT

The data that support the findings of this study are available from the corresponding author upon reasonable request.

REFERENCES

[1]L. Deike, W. K. Melville, and S. Popinet, "Air entrainment and bubble statistics in breaking waves," Journal of Fluid Mechanics **801**, 91–129 (2016).

[2]N. Kantarci, F. Borak, and K. O. Ulgen, "Bubble column reactors," Process Biochemistry **40**, 2263–2283 (2005).

[3]J. Sadighi Dizaji, "Heat transfer enhancement due to air bubble injection into a horizontal double pipe heat exchanger," Automotive Science and Engineering **4** (2014).

[4]M. Schlüter, S. Herres-Pawlis, U. Nieken, U. Tuttlies, and D. Bothe, "Small-scale phenomena in reactive bubbly flows: Experiments, numerical modeling, and applications," Annual Review of Chemical and Biomolecular Engineering **12**, 625–643 (2021).

[5]S. Sarkar and R. P. Selvam, "Direct Numerical Simulation of Heat Transfer in Spray Cooling Through 3D Multiphase Flow Modeling Using Parallel Computing," Journal of Heat Transfer **131** (2009).

[6]Y. Shirai, M. Wakisaka, O. Miyawaki, and S. Sakashita, "Effect of seed ice on formation of tube ice with high purity for a freeze wastewater treatment system with a bubble-flow circulator," Water Research **33**, 1325–1329 (1999).

[7]L. Wang, H.-G. Lee, and P. Hayes, "A new approach to molten steel refining using fine gas bubbles," ISIJ International **36**, 17–24 (1996).

[8]M. C. Boufadel, S. Socolofsky, J. Katz, D. Yang, C. Daskiran, and W. Dewar, "A review on multiphase underwater jets and plumes: Droplets, hydrodynamics, and chemistry," Reviews of Geophysics **58**, e2020RG000703 (2020).

[9]D. Bhaga and M. Weber, "In-line interaction of a pair of bubbles in a viscous liquid," Chemical Engineering Science **35**, 2467–2474 (1980).

[10]J. Katz and C. Meneveau, "Wake-induced relative motion of bubbles rising in line," International Journal of Multiphase Flow **22**, 239–258 (1996).

[11]M. Watanabe and T. Sanada, "In-line motion of a pair of bubbles in a viscous liquid," JSME International Journal Series B Fluids and Thermal Engineering **49**, 410–418 (2006).

[12]T. Sanada, A. Sato, M. Shirota, and M. Watanabe, "Motion and coalescence of a pair of bubbles rising side by side," Chemical Engineering Science **64**, 2659–2671 (2009).

[13]H. Kusuno and T. Sanada, "Experimental investigation of the motion of a pair of bubbles at intermediate reynolds numbers," Multiphase Science and Technology **27**, 51–66 (2015).

[14]H. Kusuno, H. Yamamoto, and T. Sanada, "Lift force acting on a pair of clean bubbles rising in-line," Physics of Fluids **31**, 072105 (2019).

[15]H. Yuan and A. Prosperetti, "On the in-line motion of two spherical bubbles in a viscous fluid," Journal of Fluid Mechanics **278**, 325–349 (1994).

[16]L. Chen, S. V. Garimella, J. A. Reizes, and E. Leonardi, "Motion of interacting gas bubbles in a viscous liquid including wall effects and evaporation," Numerical Heat Transfer, Part A Applications **31**, 629–654 (1997).

[17]N. Hasan and Z. binti Zakaria, "Computational approach for a pair of bubble coalescence process," International Journal of Heat and Fluid Flow **32**, 755–761 (2011).

[18]R. Chen, W. Tian, G. Su, S. Qiu, Y. Ishiwatari, and Y. Oka, "Numerical investigation on coalescence of bubble pairs rising in a stagnant liquid," Chemical Engineering Science **66**, 5055–5063 (2011).

[19]M. Tripathi, P. A Ram, K. Sahu, and R. Govindarajan, "Two initially spherical bubbles rising in quiescent liquid," Physical Review Fluids **2** (2017).

[20]Y. Zhang, K. Chen, Y. You, and W. Ren, "Coalescence of two initially spherical bubbles: Dual effect of liquid viscosity," International Journal of Heat and Fluid Flow **72**, 61–72 (2018).

[21]Y. Cao and R. Macián-Juan, "The wobbling motion of single and two inline bubbles rising in quiescent liquid," Physics of Fluids **33**, 073305 (2021).

[22]A. Kumar, B. Ray, and G. Biswas, "Dynamics of two coaxially rising gas bubbles," Physics of Fluids **33**, 052106 (2021).

[23]J. R. Vélez-Cordero, D. Sámano, P. Yue, J. J. Feng, and R. Zenit, "Hydrodynamic interaction between a pair of bubbles ascending in shear-thinning inelastic fluids," Journal of Non-Newtonian Fluid Mechanics **166**, 118–132 (2011).

[24]W. Fan and X. Yin, "Numerical study on interaction between two bubbles rising side by side in cmc solution," Chinese Journal of Chemical Engineering **21**, 705–713 (2013).

[25]M. T. Islam, P. Ganesan, and J. Cheng, "A pair of bubbles' rising dynamics in a xanthan gum solution: a cfd study," RSC Adv. **5**, 7819–7831 (2015).

[26]J. Liu, C. Zhu, X. Wang, T. Fu, Y. Ma, and H. Li, "Three-dimensional numerical simulation of coalescence and interactions of multiple horizontal bubbles rising in shear-thinning fluids," AIChE Journal **61**, 3528–3546 (2015).

[27]W. Sun, C. Zhu, T. Fu, Y. Ma, and H. Li, "3d simulation of interaction and drag coefficient of bubbles continuously rising with equilateral triangle arrangement in shear-thinning fluids," International Journal of Multiphase Flow **110**, 69–81 (2019).

[28]W. Sun, C. Zhu, T. Fu, Y. Ma, and H. Li, "Interaction and drag coefficient of three horizontal bubbles with different sizes rising in the shear-thinning fluids," International Journal of Multiphase Flow **125**, 103214 (2020).

[29]Y. Bao, J. Jia, S. Tong, Z. Gao, and Z. Cai, "A review on single bubble gas–liquid mass transfer," Chinese Journal of Chemical Engineering **28**, 2707–2722 (2020).

[30]L. Zhang, C. Yang, and Z.-S. Mao, "Numerical simulation of a bubble rising in shear-thinning fluids," Journal of Non-Newtonian Fluid Mechanics **165**, 555–567 (2010).

[31]A. Premlata, M. K. Tripathi, B. Karri, and K. C. Sahu, "Numerical and experimental investigations of an air bubble rising in a carreau-yasuda shear-thinning liquid," Physics of fluids **29**, 033103 (2017).

[32]J. C. Cano-Lozano, C. Martínez-Bazán, J. Magnaudet, and J. Tchoufag, "Paths and wakes of deformable nearly spheroidal rising bubbles close to the transition to path instability,"

Phys. Rev. Fluids **1**, 053604 (2016).

[33]J. Brackbill, D. Kothe, and C. Zemach, "A continuum method for modeling surface tension," Journal of Computational Physics **100**, 335–354 (1992).

[34]K. Yasuda, R. C. Armstrong, and R. E. Cohen, "Shear flow properties of concentrated solutions of linear and star branched polystyrenes," Rheologica Acta **20**, 163–178 (1981).

[35]S. Popinet, "Solitary wave run-up on a plane beach," `http://basilisk.fr/src/test/beach-ml.c` (2019).

[36]P. Karnakov, S. Litvinov, and P. Koumoutsakos, "A hybrid particle volume-of-fluid method for curvature estimation in multiphase flows," International Journal of Multiphase Flow **125**, 103–209 (2020).

[37]J. López-Herrera, S. Popinet, and A. Castrejón-Pita, "An adaptive solver for viscoelastic incompressible two-phase problems applied to the study of the splashing of weakly viscoelastic droplets," Journal of Non-Newtonian Fluid Mechanics **264**, 144–158 (2019).

[38]S. Popinet, "An accurate adaptive solver for surface-tension-driven interfacial flows," Journal of Computational Physics **228**, 5838–5866 (2009).

[39]K. Kazemi, A. Vernet, F. X. Grau, S. Cito, and A. Fabregat, "Passive scalar transfer rate at bubble interface in carreau liquid in a transition regime," International Journal of Multiphase Flow **150**, 104000 (2022).

[40]G. Brereton and D. Korotney, "Coaxial and oblique coalescence of two rising bubbles," Dynamics of bubbles and vortices near a free surface **119**, 50–73 (1991).

[41]I. Chakraborty, G. Biswas, and P. Ghoshdastidar, "A coupled level-set and volume-of-fluid method for the buoyant rise of gas bubbles in liquids," International Journal of Heat and Mass Transfer **58**, 240–259 (2013).

[42]D. Bhaga and M. E. Weber, "Bubbles in viscous liquids: shapes, wakes and velocities," Journal of Fluid Mechanics **105**, 61–85 (1981).

[43]R. Clift, J. R. Grace, and M. E. Weber, "Bubbles, drops, and particles," (Courier Corporation, 2005).

[44]M. Tripathi, K. Sahu, and R. Govindarajan, "Dynamics of an initially spherical bubble rising in quiescent liquid," Nature communications **6**, 6268 (2015).

[45]D. Colombet, D. Legendre, A. Cockx, and P. Guiraud, "Mass or heat transfer inside a spherical gas bubble at low to moderate reynolds number," International Journal of Heat and Mass Transfer **67**, 1096–1105 (2013).

[46]G. Juncu, "A numerical study of the unsteady heat/mass transfer inside a circulating sphere," International Journal of Heat and Mass Transfer **53**, 3006–3012 (2010).

[47]M. J. M. Hill, "Vi. on a spherical vortex," Philosophical Transactions of the Royal Society of London.(A.) , 213–245 (1894).

[48]I. Lashgari, J. O. Pralits, F. Giannetti, and L. Brandt, "First instability of the flow of shear-thinning and shear-thickening fluids past a circular cylinder," Journal of Fluid Mechanics **701**, 201–227 (2012).

[49]M. Roudet, A.-M. Billet, S. Cazin, F. Risso, and V. Roig, "Experimental investigation of interfacial mass transfer mechanisms for a confined high-reynolds-number bubble rising in a thin gap," AIChE Journal **63** (2016).